AFRL-RX-WP-TP-2011-4223

CREEP, PLASTICITY, AND FATIGUE OF SINGLE CRYSTAL SUPERALLOY

Alexander Staroselsky

United Technologies Corporation
Pratt & Whitney

Brice N. Cassenti

University of Connecticut

JULY 2011

Approved for public release; distribution unlimited.

See additional restrictions described on inside pages

STINFO COPY

AIR FORCE RESEARCH LABORATORY
MATERIALS AND MANUFACTURING DIRECTORATE
WRIGHT-PATTERSON AIR FORCE BASE, OH 45433-7750
AIR FORCE MATERIEL COMMAND
UNITED STATES AIR FORCE

REPORT DOCUMENTATION PAGE

Form Approved
OMB No. 0704-0188

The public reporting burden for this collection of information is estimated to average 1 hour per response, including the time for reviewing instructions, existing data sources, gathering and maintaining the data needed, and completing and reviewing the collection of information. Send comments regarding this burden estimate or any other aspect of this collection of information, including suggestions for reducing this burden, to Department of Defense, Washington Headquarters Services, Directorate for Information Operations and Reports (0704-0188), 1215 Jefferson Davis Highway, Suite 1204, Arlington, VA 22202-4302. Respondents should be aware that notwithstanding any other provision of law, no person shall be subject to any penalty for failing to comply with a collection of information if it does not display a currently valid OMB control number. **PLEASE DO NOT RETURN YOUR FORM TO THE ABOVE ADDRESS**.

1. REPORT DATE *(DD-MM-YY)* July 2011	**2. REPORT TYPE** Journal Article Preprint	**3. DATES COVERED *(From - To)*** 01 July 2011 – 01 July 2011

4. TITLE AND SUBTITLE
CREEP, PLASTICITY, AND FATIGUE OF SINGLE CRYSTAL SUPERALLOY

5a. CONTRACT NUMBER
FA8650-07-C-5252

5b. GRANT NUMBER

5c. PROGRAM ELEMENT NUMBER
62102F

6. AUTHOR(S)
Alexander Staroselsky (United Technologies Corporation, Pratt & Whitney)
Brice N. Cassenti (University of Connecticut)

5d. PROJECT NUMBER
4347

5e. TASK NUMBER
20

5f. WORK UNIT NUMBER
24110202

7. PERFORMING ORGANIZATION NAME(S) AND ADDRESS(ES)

United Technologies Corporation
Pratt & Whitney
400 Main St., MS165-16
East Hartford, CT 06108

University of Connecticut
191 Auditorium Road, U-3139
Storrs, CT 06269-3139

8. PERFORMING ORGANIZATION REPORT NUMBER

9. SPONSORING/MONITORING AGENCY NAME(S) AND ADDRESS(ES)

Air Force Research Laboratory
Materials and Manufacturing Directorate
Wright-Patterson Air Force Base, OH 45433-7750
Air Force Materiel Command
United States Air Force

10. SPONSORING/MONITORING AGENCY ACRONYM(S)
AFRL/RXLM

11. SPONSORING/MONITORING AGENCY REPORT NUMBER(S)
AFRL-RX-WP-TP-2011-4223

12. DISTRIBUTION/AVAILABILITY STATEMENT
Approved for public release; distribution unlimited.

13. SUPPLEMENTARY NOTES
PAO case number 88ABW-2010-2393 cleared 03 May 2010. This work was funded in whole or in part by Department of the Air Force contract FA8650-07-C-5252. The U.S. Government has for itself and others acting on its behalf an unlimited, paid-up, nonexclusive, irrevocable worldwide license to use, modify, reproduce, release, perform, display, or disclose the work by or on behalf of the U. S. Government. Submitted to the International Journal of Solids & Structures. Document contains color.

14. ABSTRACT

Single crystal components in gas turbine engines are subject to such extreme temperatures and stresses that life prediction becomes highly inaccurate resulting in components that can only be shown to meet their requirements through experience. Reliable life prediction methodologies are required both for design and life management. In order to address this issue we have developed a thermo-viscoplastic constitutive model for single crystal materials. Our incremental large strain formulation additively decomposes the inelastic strain rate into components along the octahedral and cubic slip planes. We have developed a crystallographic–based creep constitutive model based on Orowan's law and applied specifically to sigmoidal creep behavior. Inelastic shear rate along each slip system is expressed as a sum of a time dependent creep component and a rate independent plastic component. We develop a new robust and computationally efficient rate-independent crystal plasticity formulation and combined it with creep flow rule calibrated for Ni-based superalloys.

15. SUBJECT TERMS
single crystal, life prediction, life management, thermo-viscoplastic, crystallographic-based creep

16. SECURITY CLASSIFICATION OF:			**17. LIMITATION OF ABSTRACT:**	**18. NUMBER OF PAGES**	**19a. NAME OF RESPONSIBLE PERSON** (Monitor)
a. REPORT	**b. ABSTRACT**	**c. THIS PAGE**	SAR	42	Andrew Rosenberger
Unclassified	Unclassified	Unclassified			**19b. TELEPHONE NUMBER** *(Include Area Code)* N/A

Standard Form 298 (Rev. 8-98)
Prescribed by ANSI Std. Z39-18

Creep, Plasticity, and Fatigue of Single Crystal Superalloy

Alexander Staroselsky[1]* and Brice N. Cassenti[2]

Abstract

Single crystal components in gas turbine engines are subject to such extreme temperatures and stresses that life prediction becomes highly inaccurate resulting in components that can only be shown to meet their requirements through experience. Reliable life prediction methodologies are required both for design and life management. In order to address this issue we have developed a thermo-viscoplastic constitutive model for single crystal materials. Our incremental large strain formulation additively decomposes the inelastic strain rate into components along the octahedral and cubic slip planes. We have developed a crystallographic–based creep constitutive model based on Orowan's law and applied specifically to sigmoidal creep behavior. Inelastic shear rate along each slip system is expressed as a sum of a time dependent creep component and a rate independent plastic component. We develop a new robust and computationally efficient rate-independent crystal plasticity formulation and combined it with creep flow rule calibrated for Ni-based superalloys. The transient variation of each of the inelastic components includes a back stress for kinematic hardening and latent hardening parameters to account for the stress evolution with inelastic strain as well as the evolution for dislocation densities. The complete formulation accurately predicts both monotonic and cyclic tests at different crystallographic orientations for constant and variable temperature conditions (low cycle fatigue (LCF) and thermo-mechanical fatigue (TMF) tests). Based on the test and modeling results we formulate a new life prediction criterion suitable for both LCF and TMF conditions.

---

[1] Pratt & Whitney, 400 Main Street, MS 165-16, East Hartford, CT 06108

[2] University of Connecticut, 191 Auditorium Rd. U-3139, Storrs, CT 06269-3139

* Corresponding Author; e-mail: Alexander.Staroselsky@pw.utc.com

Introduction

Failure is a localized process evolving in time and leading to global structure instabilities when a limiting state is met. This paper describes how the material properties and loading affects the damage initiation and propagation. High temperature superalloy material damage is most closely tied to crystallographic slip along definite crystallographic planes. Among micromechanical deformation mechanisms, slip along crystallographic planes controls the evolution of the microstructure in materials, and in turn, leads to failure. Energy dissipation in a loaded structure could take place either by plastic deformation or by microcracking. Although materials plasticity decreases structure susceptibility to the cracking, when the density of plastic defects becomes too high, secondary cracking might be initiated. Under applied stress, slip bands run into each other, generating new dislocations and also forming a dislocation pile up next to an obstacle. This means that slip bands intersection may result in the appearance of cracks.

We studied the micromechanics of the high temperature creep, plasticity, and damage accumulation in single crystal nickel base superalloy. These alloys are used in turbine blade and vane applications in advanced commercial and military gas turbines and in the turbopumps for the space shuttle main engines. Significant progress in airfoil design led to development of thin hollow air-cooled and film-cooled blades reducing the alloy temperature. However, this process causes high temperature gradients in the blade making local creep and thermo-mechanical fatigue (TMF) a problem that is crucial in the proper blade damage tolerant design (Cowles, 1996). The final objective of such a study ultimately should be the development of a robust predictive tool to relate single crystal structure macroscopic behavior and fracture crack initiation to micromechanical events (Rubeša, 1996). Modern blade design still relies mostly on empirical approaches, because the nonlinear cyclic visco-plastic structural analysis for single crystal blades requires advanced material constitutive and damage evolution models that still have not reached maturity and are computationally expensive. Historically, only secondary creep effects were considered (e.g., Larson-Miller, etc.) in engineering calculations. However, during thermo-mechanical loading of high temperature single crystal turbine parts, all three creep stages: primary, secondary and tertiary, manifest themselves and none of them can be neglected (Epishin and Link (2004), Staroselsky and Cassenti (2006)). Account must be taken of all creep mechanisms, and is especially important in the case of non-homogeneous thermal loading of components with extensive stress redistribution and relaxation. We have developed a unified materials constitutive model including thermally-dependent creep activation mechanisms for different crystallographic orientations. The model extends existing approaches (Nissley et al. 1991, Cuitino and Ortiz M. 1993, C. Allen 1995) to increase the accuracy of elastic-visco-plastic material deformation response predictions for cyclic and thermal-cyclic loading. We have experimentally observed and simulated, with our unified microstructure-based model, loading cases with only primary and tertiary creep regimes (no secondary creep) as well as creep without any noticeable primary creep. The approach used in simulations of the deformation process of $L1_2$ single crystal gives us a tool to obtain the deformation behavior of these structures (Staroselsky and Cassenti 2008).

The purpose of this work is to predict stress-strain evolution and crystallographic lattice re-orientation during finite visco-plastic deformation. We also aim to evaluate low cycle and thermal fatigue life for generic non-isothermal cyclic loading to simulating typical portions of aircraft engine mission. For such a purpose we need to analyze combined creep and plastic regimes, concentrating on cyclic plasticity effects. Low cycle fatigue (LCF) as well as TMF are cyclic plasticity (inelasticity) driven processes. Therefore, we concentrate on combined plasticity and creep deformation predictions. In such a regime, long time dwell effects follow high stress but relatively short periods of elastic-plastic deformation. From a modeling standpoint, we have to decompose the inelastic deformation (or inelastic velocity gradient) into plastic and creep (i.e., high rate sensitive viscous) deformation. Hence, the possible rate dependent nature of the plastic part of the flow rule will interfere with creep predictions ultimately resulting in numerical errors. Typical creep and creep/fatigue tests last hundreds of hours but our numerical experiments with a plastic model rate sensitivity of 0.03 (n=33) demonstrated that even this low rate sensitivity significantly affects the strain behavior after about 300 hours of tests. This strain might be eliminated by increasing the exponent to the level of 100 or even 250 and higher, as shown in (Pierce et al 1983, Needleman 1988, Kalidindi and Anand, 1994) but this leads to stiff numerical equations with their corresponding computational difficulties. It is also important to note that the rate sensitivity of Ni-based superalloys is small, which in turn leads to high values of the exponent, *n*. The alternative and numerically efficient way of accounting for plasticity is to develop a rate-independent model which can be easily combined with creep terms. Some of the earliest time independent formulations were proposed by Kremple (1976), Valanis (1976), Walker (1980), Cassenti (1983), Pierce et al 1982, and Chaboche (1986). However, the rate-independent model should be free of limitations inherent in the rate-independent idealization. One of them is the long standing problem of the loss of uniqueness of the choice of active slip systems and slip increments. Our new general approach for rate independent plasticity formulation uses the idea that the plastic strain rate is proportional to an energy rate and ultimately cancelling the time differential in the denominators of derivatives, resulting in a rate-independent formulation. Both isotropic and kinematic hardening are included using the time dependent formulation. Our rate-independent formulation combines the advantages of the rate dependent power law and the numerical efficiency of rate independent approach. As will be shown in this paper we relate slip systems shear increments with the effective shear stresses acting along these systems thus uniquely defining an incremental solution. We verified our formulation by making it agree exactly with a rate dependent plastic formulation with low rate sensitivity (n=100). In this paper we in particular focus on the development of a generic rate-independent crystal plasticity model suitable for cyclic non-isothermal elastic-plastic-viscoplastic analysis.

The final goal of the constitutive modeling is to predict the expected life and the failure modes of single crystal components. Although we should develop a framework for such an analysis, unfortunately it is beyond the scope of this paper. However, our model is the perfect tool for the prediction of shear localization leading in turn to the material failure. Mathematically, shear localization corresponds to the loss of ellipticity of the governing equations (Rice and Rudnicki 1980, J. Schröder 2004). It was shown (Needleman, 1989) that rate sensitivity affects the stress-strain behavior and precludes shear band formation. In our rate-independent plasticity model there is no abrupt change in model behavior with increases in the stress. Due to the fact that this model can be combined with a broad range of hardening relations it makes this framework an important tool for generic static and dynamic materials deformation predictions and stability analysis.

Summarizing, we have developed and examined in detail a creep model predicting so-called sigmoidal (V. Levitin, 2006) creep for a broad temperature range for superalloy applications and combine it with a new plasticity formulation that is time independent but does not possess a yield surface. This is very important for the analysis of stress – strain distribution due to significant temperature changes. At high temperatures creep is the dominant mode of deformation and because of stress redistribution the applied stress levels remain at moderate levels and do not result in plastic deformation. However, after the cooling creep deformation simply disappears and inelastic deformation takes place by plasticity which does not vary with temperature as strongly as creep. Our creep experiments show that creep rates follow an Arrhenius type relationship with the value of the activation energy varying slightly around $Q = 7.0E-19\ J/atom$ with some increase of the activation energy for the temperatures below 700 C. Hence plasticity plays a major role in residual stress generation after cooling during cyclic thermal loading.

The prediction of component fatigue life is based on empirical or semi-empirical relationships, (for example, the widely used SWT relation described in Smith et al. 1970) requiring the knowledge of detailed stress - strain variation with time as well as the time evolution of damage parameters. The advanced constitutive model is an indispensable tool for stress-strain analysis during transient structural analysis and for the accurate sub-modeling of the part of the structure susceptible to the excessive temperatures and/or loads. The appropriate model should be able to reproduce the observed hysteresis loops (Rubeša, 1996), stress evolution and redistribution. The hysteresis loop evolution due to latent and kinematic hardening, strain ratcheting under loading with non-zero mean axial stress (Abdel-Karim and Ohno, (2000), Bari and Hassan (2000)), and the stress-strain loop stabilization are probably the most important phenomena observed during LCF and TMF. For example, ratcheting accelerates damage accumulation and reduces the fatigue life. During out of phase TMF tests, ratcheting leads to significant increases of the tensile stresses at low temperature eventually causing specimen cracking. While the low temperature materials response can be modeled by rate-independent plasticity, high temperature creep is essentially rate-dependent causing additional stress relaxation affecting cyclic hysteresis loop. Defining fatigue as an inelasticity driven process of cyclic damage accumulation, we have to be able accurately predict stress and strain variation in a cycle as well as overall cycles evolution during service. In order to achieve this, we verify our constitutive model predictions for cyclic isothermal and non-isothermal tests over a broad range of boundary conditions and single crystal crystallographic orientations. Based on calculated stress-strain hysteresis loops and measured LCF and TMF cycles to failure we propose a simple life model which can be used to predict both LCF and TMF cycles to failure for Ni-based superalloys.

The constitutive model has been implemented in the commercial finite element software ANSYS as a material user routine. The model is calibrated against stress-strain and crystallographic texture predictions using creep and plasticity test data up to 25% strain. Our non-isothermal, crystal elastic–visco-plastic model can used to predict the stress and strain distribution, cyclic ratcheting and the residual stress accumulation needed for life prediction due to LCF and TMF conditions.

The plan of the paper is as follows: In the next section we review the basic governing equations. After this, we formulate the transient creep flow rule representing high temperature behavior of single crystal Ni-based superalloys. In the section 4 we propose the new rate-independent plasticity formulation and also verify it for a few examples. The combined evolution model is applied to a number of isothermal and thermal-mechanical fatigue loading conditions and results are verified against original test data in section 5. In section 6 we formulate a life prediction model and apply it to forty LCF and TMF coupon test results. We close with some discussion and some final remarks.

2. Governing Equations

The deformation of a crystal is taken as the sum of contributions from an overall elastic distortion of the lattice and generalized inelastic deformation. The governing variables in the constitutive model are taken as: (1) the Cauchy stress **T,** (2) the deformation gradient, **F** and (3) plastic deformation gradient $\mathbf{F^p}$ with det$\mathbf{F^p}$ =1. Each crystal slip system is specified by a unit normal $\mathbf{n}_0^{\alpha}$ to the slip plane, and a unit vector $\mathbf{m}_0^{\alpha}$ denoting the slip direction. Generalized inelastic deformation is maintained through the twelve octahedral slip systems <110>(111) and the six cube slip systems <110>(001) that also contributing to the visco-plastic flow of Ni based superalloys tt high temperatures. The material model parameters are different for the octahedral and cube slip systems.

Kinematics

The elastic deformation gradient is defined by decomposition of the total deformation gradient as follows: $\mathbf{F} = \mathbf{F^e F^{in}}$ and $\det \mathbf{F^e} > 0$. $\mathbf{F^e}$ describes the elastic distortion of the lattice; and gives rise to the stress **T**. For metallic materials the constitutive equation for the second Piola-Kirchhoff stress tensor is taken as a linear relation

$$\begin{aligned} \mathbf{T^*} &= \mathbf{C}[\mathbf{E^*} - \mathbf{A}\cdot(\Theta - \Theta_0)] \\ \mathbf{E^*} &= \tfrac{1}{2}\left[\mathbf{F^{eT}F^e} - \mathbf{1}\right] \end{aligned} \qquad (2)$$

where **A** - is the rank two thermal extension tensor

C – is the temperature dependent anisotropic elasticity tensor, Θ is the temperature and Θ_0 is the reference temperature. The elastic strain measure is the Cauchy-Green tensor. The Cauchy Stress tensor is the work-conjugate stress corresponding to the Cauchy-Green strain elastic measure and is calculated as follows:

$$\mathbf{T} = \frac{1}{\det(\mathbf{F^e})}\mathbf{F^e T^* F^{eT}} \tag{3}$$

The evolution equation for the viscoplastic deformation gradient is given by the flow rule:

$$\begin{aligned} \dot{\mathbf{F}}^{in} &= \mathbf{L}^{in}\mathbf{F}^{in} \\ \mathbf{L}^{in} &= \sum_{slip\ systems} \dot{\gamma}^{\alpha}\mathbf{S}^{\boldsymbol{\alpha}} \qquad \mathbf{S}^{\boldsymbol{\alpha}} = \mathbf{m}^{\boldsymbol{\alpha}} \otimes \mathbf{n}^{\boldsymbol{\alpha}} \end{aligned} \tag{4}$$

The shear rate along each slip system $\dot{\gamma}^{\alpha}$ is given in terms of the resolved shear stress (RSS) $\tau = \mathbf{T}^* \bullet \mathbf{S}^{\boldsymbol{\alpha}}$, slip systems resistances and equilibrium stress (or back stress). Expression (4) has the incremental flow rule form as follows:

$$\mathbf{F}^{in}(\tau) = \mathbf{L}^{in}(\tau)\mathbf{F}^{in}(t) = (\mathbf{1} + \sum_{\alpha} \Delta\gamma^{\alpha}\mathbf{S}_{\mathbf{0}}^{\boldsymbol{\alpha}})\mathbf{F}^{in}(t) \tag{5}$$

We decompose the deformation velocity into creep and plasticity parts as follows:

$$\mathbf{L^{in}} = \mathbf{L^p} + \mathbf{L^c} \tag{6}$$

combining creep deformation and rate independent plastic deformation. At each time both the plastic and creep deformation increments depend on the cumulative inelastic deformation gradient achieved by this time. If we additionally specify that both creep and plastic deformations take place by slip along specified slip systems, then the total slip increment can be decomposed in the following way:

$$\Delta\gamma^{\alpha} = \Delta\gamma^{\alpha}_{plastic} + \Delta\gamma^{\alpha}_{creep}. \tag{7}$$

Evolution of crystallographic texture is explicitly defined by the elastic part of the deformation gradient.

$$\begin{aligned} \mathbf{m}_{\mathbf{t}}^{\boldsymbol{\alpha}} &= \mathbf{F^e m}_{\mathbf{0}}^{\boldsymbol{\alpha}} \\ \mathbf{n}_{\mathbf{t}}^{\boldsymbol{\alpha}} &= \mathbf{F}^{\mathbf{e}^{-\mathbf{T}}} \mathbf{n}_{\mathbf{0}}^{\boldsymbol{\alpha}} \end{aligned} \tag{8}$$

This paper focuses its attention on high temperature deformation, where the octahedral and cube slip systems are the major deformation mechanisms. Possible contributions from other slip and twin systems, sometimes observed at low temperatures, are not within the scope of this paper. In order to complete the governing equations we have to formulate specific flow rules for creep and plasticity.

3. Flow rule for creep

We use viscoplastic models to represent the macroscopic mechanical response of the single crystal material. An increase in the density of mobile dislocations causes a rapid rise in the creep deformation rate $\dot{\gamma}^{c}$. In turn this leads to tertiary creep, and can reduce or even eliminate the secondary creep stage. Such a behavior is often observed in Ni-based superalloys and sometimes referred to as sigmoidal creep. This dislocation driven mechanism does not directly affect crystallographic structure or material elastic properties. In order to describe these observations, we use Orowan's assumption that the creep strain rate is proportional to the density of the mobile dislocations, ρ_m. If we denote an arbitrary reference dislocation density throughout as ρ_0, then the dimensionless parameter $\frac{\rho_m}{\rho_0}$ serves as a measure of the mobile dislocation density, and can be used to predict tertiary creep. We have used a standard viscoplastic power law creep with a back stress (Nissley *et al.* 1991) to represent the response of the material. The constitutive law for the creep strain rate along α–th slip system, $\dot{\gamma}^{\alpha}_{\sec}$ is written as follows:

$$\dot{\gamma}^{\alpha}_{\sec} = \dot{\gamma}_0 \left(\frac{\rho^{\alpha}_{m}}{\rho_0}\right) \left|\frac{\tau^{\alpha} - \omega^{\alpha}}{s^{\alpha}}\right|^{n} \operatorname{sgn}\left(\tau^{\alpha} - \omega^{\alpha}\right) \exp\left(-\frac{Q}{kT}\right), \tag{9}$$

where $\dot{\gamma}_0$ is a (generally speaking, temperature dependent) time constant, s^{α} is the deformation resistance of α-th slip system, and τ^{α} is the resolved shear stress. Our creep experiments show that creep rates follow an Arrhenius type relationship with the value of the activation energy varying in the range from $Q_{oct>} = 6.97E-19$ to for octahedral slip systems to $Q_{cube>} = 7.30E-19 \quad J/atom$ for cube slip systems for the temperatures above 700 C. State variable ω^{α} is the slip system back stress representing kinematic hardening, *n* is the creep exponent set to be equal to 3 in these simulations, and $(\dot{\ })$ is the rate of change with respect to time.

We have chosen the evolution of latent hardening to be described by a modified Asaro rule (Asaro 1983) $\dot{s}^{\alpha} = h_0 \left(1 - \frac{s^{\alpha}}{s^{*}}\right)^{p} \sum_{\beta} h^{\alpha\beta} \left|\dot{\gamma}^{\beta}\right|$, with temperature dependent parameters and a hardening matrix $h^{\alpha\beta} = \left\{q + (1-q)\delta^{\alpha\beta}\right\}$ and $q = 1.4$. It will be shown later in this paper that accounting for temperature dependence of the initial slip resistance s_0 is crucial for the simulation of thermal mechanical fatigue (TMF). As one can see the latent hardening is a monotonic saturating function with respect to accumulated inelastic strain.

Kinematic hardening (back stress) evolves according to the following relationship (Nissley *et al.* 1991, Stouffer and Dame 1996)

$$\dot{\omega}^{\alpha} = \lambda\left(\dot{\gamma}^{\alpha} - \omega_{\infty}\left|\dot{\gamma}^{\alpha}\right|\omega^{\alpha}\right) \tag{10}$$

The back stress also has a limiting saturation value, ω_{∞}, corresponding to the end of the primary creep stage. The back stress requires two additional coefficients λ and ω_{∞} that are explicit functions of temperature. It is important to note that hardening terms indirectly account for rafting processes and for the microstructure evolution during the first stage of creep.

To complete the formulation of the creep constitutive model we need to define the evolution equations for the dislocation density. Dislocation generation and motion represents a non-recoverable state for the material. These states can be related to the energy for the system through equilibrium statistical mechanics. We postulate that dislocation generation rate is proportional to the rate of entropy production which can be expressed by

$$\dot{S} = C\sum_{i=1}^{n_{slip}}\left(\frac{\tau^{i} - \omega^{i}}{s}\right)\dot{\gamma}^{i} \geq 0, \qquad (11)$$

where the parameter C is a constant, and n_{slip} is the number of active slip systems.
In this model we consider two types of the dislocations: mobile and pinned with densities evolving over time. We have chosen to use concepts from chemical kinetics to represent the dislocation evolution as two body interactions. We assume that dislocation immobilization takes place when two corresponding dislocation loops interact with each other. Taking into account that $\dot{\gamma}^{\alpha}$ is already a linear function of the mobile dislocation density to represent two body interactions we immediately obtain relations for mobile and pinned dislocations evolution along each slip system:

$$\begin{aligned}
\dot{\rho}_{m}^{\alpha} &= M\left(\frac{\tau^{\alpha} - \omega^{\alpha}}{s^{\alpha}}\right)\dot{\gamma}^{\alpha}\left(\frac{\varepsilon^{2}\rho_{m}^{ss} + \rho_{p}^{ss} - \rho_{p}^{\alpha} - \varepsilon^{2}\rho_{m}^{\alpha}}{\rho_{0}}\right) \\
\dot{\rho}_{p} &= \Pi\left(\frac{\tau^{\alpha} - \omega^{\alpha}}{s^{\alpha}}\right)\dot{\gamma}^{\alpha}\left(\frac{\rho_{p}^{ss} - \rho_{p}^{\alpha}}{\rho_{0}}\right)
\end{aligned} \qquad (12)$$

where M and Π represent specific time constants, that are different for octahedral and cube slip systems. A normalized plot of these parameters against temperature is shown in Fig 1, ρ_{m}^{ss} , is the saturated mobile dislocation density, ρ_{p}^{ss} , is the saturated pinned dislocation density, and ε^{2} is a positive weight constant. Equations (12) include the generation of mobile dislocations and also include their conversion to pinned dislocations. The dislocation density evolution governed by the differential equations (12) allows for the prediction of exponential type creep strain behavior, specific for Ni-based superalloys of $L1_2$ crystallographic structure. The maximum value of the back stress ω_{∞} for cube systems is much higher at low temperatures and drops rapidly with the temperature increase as shown in Fig 2. This change together with the rapid decrease of the latent hardening cube slip resistance with temperature shows the increasingly important role of cube systems at high temperature and their very limited effect on inelastic deformation at low temperatures.

During the early stage of creep, dislocation nucleation and dislocation motion are the principal creep deformation mechanism (Sugui et al. (1999), Rae et al. 2007). Dislocation loops move mostly in the matrix channels (Pollock and Argon (1992)) maintaining the generalized plastic flow. Thus, dislocations cross-slip causes strain hardening which in turn decreases the rate of creep deformation. Increases in the dislocation density and in the number of dislocation pile-ups makes further deformation more and more difficult, resulting in the transition of creep from the primary stage to a secondary one.

In order to predict primary creep in Ni-based superalloys, we have developed a rate-dependent crystal plasticity formalism with a threshold stress on each slip system. Since dislocation strengthening is proportional to the square root of the dislocation density (for example, U. Kocks (1976) , H. Mughrabi 1975), we take the threshold value to also be proportional to the square root of the total dislocation density. The threshold stress reflects the resistance to plastic flow arising from hardening associated with an increase of dislocation density and cross-slip. All threshold parameters as well as hardening parameters depend on temperature.

$$\dot{\gamma}^{\alpha}_{primary} = \dot{\gamma}_0 \left\langle \frac{\left(\tau^{\alpha} - \omega_p{}^{\alpha}\right) - \kappa\sqrt{\rho^{\alpha}_{p}}}{s^{\alpha}} \right\rangle^{n} \operatorname{sgn}\left(\frac{\tau^{\alpha} - \omega_p{}^{\alpha}}{s^{\alpha}}\right) \exp\left(-\frac{Q}{kT}\right) \qquad (13)$$

Where $\langle a \rangle = \begin{cases} a & \text{if } a > 0 \\ 0 & \text{if } a \le 0 \end{cases}$ and κ is temperature dependent fitting parameter.

In the formula for the back stress, parameter λ is a characteristic time parameter describing how fast the back stress converges to its saturation value ω_{∞}. Primary creep is much faster process than secondary and tertiary stages, so this dictates a smaller value of λ while the saturation value ω_{∞} is the same for all creep stages. With an increase in primary creep deformations, dislocation density increases (see Eq. 12) thus reducing the effective stresses to very small values. Simultaneously, the hardening s also increases which effectively reduces the ratio in (13). Thus, the primary creep slip rate gradually decreases from a significant value to zero. The total creep deformation rate for each slip system is the direct sum of tertiary creep Orowan's type $\dot{\gamma}^{\alpha}_{\sec}$ expression (9) and the primary one (13) as: $\dot{\gamma}^{\alpha}_{creep} = \dot{\gamma}^{\alpha}_{primary} + \dot{\gamma}^{\alpha}_{\sec}$. Primary creep has been mainly observed in Ni-based superalloy at relatively low temperatures and high applied nominal stresses. Typical creep curves obtained at 760 C and the model predictions are shown in Fig. 3. It is very important to note that primary creep disappears with a decrease of the nominal stress. Also, the amount of primary creep is much bigger during tensile tests along the (001) crystallographic direction. The threshold parameter κ slightly decreases with temperature but due to the fast growth of dislocation multiplication rate with temperature rise, the whole term $\kappa\sqrt{\rho^{\alpha}_{p}}$ increases and effectively eliminates primary creep for the temperature range above 950 C for moderate stress levels. Very interesting results have been observed in creep tests conducted at 870 C loaded by two different nominal stresses. Primary creep was pronounced if the nominal stress was 550 MPa and no primary creep was observed if the nominal stress was 414 MPa. These creep test results together with model predictions are shown in Fig. 4. The Figures 5a and 5b illustrate model calculations versus test results for two crystallographic orientations <001> and <111> at temperatures of 982 C and 1038 C in which primary creep region is insignificant.

4. New time-independent plasticity formulation

In the previous section we have described our rate dependent (creep) model by using appropriate constitutive power laws. Many turbine parts are subject to long term viscoplastic deformations as well as time independent inelasticity caused by high stress levels. This combination of creep and plasticity leads to severe damage accumulation significantly reducing service life. In this section we formulate our new rate-independent flow rule for crystal plasticity and compare the deformation and slip activities model predictions against a classical power law. The presented formulation combines the computational benefits of rate independent plastic behavior description with the advantages of a rate dependent power method affirming the uniqueness of active slip increments calculations.

As an introduction to the method let us consider an inelastic strain, γ^p to be a single value function of N state variables, θ_i, such that $\gamma^p = f(\theta_{1,}\theta_2,\dots,\theta_N)$. The time rate of change of the inelastic strain will be given by

$$\dot{\gamma}^p = \sum_{i=1}^{N} \frac{\partial f}{\partial \theta_i} \dot{\theta}_i \, , \tag{14}$$

Please note in equation (14) that, although there are rates on both sides of the equation, the inelastic strain is not an explicit function of time. This can be seen if we consider the definition of a derivative. The denominators in each of the terms contains a time change that can be “canceled” to yield

$$d\gamma^p = \sum_{i=1}^{N} \frac{\partial f}{\partial \theta_i} d\theta_i \tag{15}$$

Equation (15) clearly shows that γ^p is not an explicit function of time. The same conclusion will hold even if the relation (15) is not an exact differential. Hence, we can write

$$\dot{\gamma}^p = \sum_{i=1}^{N} G(\theta_{1,}\theta_2,\dots,\theta_N)\dot{\theta}_i \, , \tag{16}$$

and still be assured that γ^p is not an explicit function of time or is “time independent”.

We use equation (16) to insure that the plastic strain rate is time independent by making it proportional to another rate. Let us consider, for example, a plastic strain rate that is proportional to the plastic work rate, $\dot{W}^p$, then we can write

$$\dot{\varepsilon}_{ij}^p = \frac{d\varepsilon_{ij}^p}{dt} = f(W^p)\dot{W}^p = f(W^p)\frac{dW^p}{dt} \tag{17}$$

Dividing both sides of equation (17) by $\frac{dW^p}{dt}$ we get

$$\frac{d\varepsilon_{ij}^{p}}{dW^{p}} = f\left(W^{p}\right). \tag{18}$$

Equation (18) makes ε_{ij}^{p} a function of W^{p} which is not explicitly dependent on the time, and subsequently the model can be labeled as rate independent.

.

Next, let us apply this concept to formulate a crystal plasticity rate-independent flow rule. For each of the slip systems the inelastic strain rate, $\dot{\gamma}^{\alpha}$, is a function of the effective stress for that slip system, $\tau^{\alpha} - \omega^{\alpha}$, and we could choose,

$$\dot{\gamma}^{\alpha} = \frac{\tau^{\alpha} - \omega^{\alpha}}{\left(s^{\alpha}\right)^{2}} \left| \frac{\tau^{\alpha} - \omega^{\alpha}}{s^{\alpha}} \right|^{m} \left\langle \dot{W}^{p} \right\rangle \tag{19}$$

where $\langle x \rangle$ is the unit ramp function of x and s^{α} is a temperature dependent latent hardening material parameter along slip system α. We use the ramp function to satisfy Kuhn-Tucker condition or in other words, there is no plasticity under unloading. Here we simply interpret this condition in the physical sense: if the energy is added to a material it might yield but if the energy is removed from the material ($\dot{W}^{p} < 0$) then there is no plastic deformation possible. The power law is used to limit activity of the slip systems with relatively moderate values of the effective resolved shear stress, which is much less than what is actually required for the active slip systems. Here we used the fact that power function with the argument varying from zero to unity behaves almost like a switch function for high powers where the closer to ideal switch (Heaviside function) the higher the exponent is. In such a way we use the advantage of the power model to guarantee the unique choice of active slip systems. In our case we can use values of the exponent $m \leq 30$ which guarantees good selection of slip activities and should remain free of the computational problems specific for rate-dependent power models with very high values of the exponent values.

Equation (19) has assumed that only the plastic work contributes to the plastic strain, but the total work rate may also be an important variable. Since $\dot{W}^{p} = \dot{W} - \dot{W}^{e}$, we can use a weighted sum of the total and elastic work rates by replacing the plastic work rate in equation (19) in the following way:

$$\dot{\gamma}^{\alpha} = \frac{\tau^{\alpha} - \omega^{\alpha}}{\left(s^{\alpha}\right)^{2}} \left| \frac{\tau^{\alpha} - \omega^{\alpha}}{s^{\alpha}} \right|^{m} \left\langle \dot{W} - k\left(\dot{W} - \dot{W}^{p}\right) \right\rangle \tag{20}$$

where k is a temperature dependent material parameter. The sign of the shear rate is defined by the sign of the effective resolved shear stress acting in the slip system. The total work rate is given by[3]

$$\dot{W} = \sum_{i,j} \sigma_{ij} \dot{\varepsilon}_{ij} = \sigma_{ij} \dot{\varepsilon}_{ij}, \tag{21}$$

and the plastic work rate is

---

[3] Equation (21) can be readily extended to large deformation formalism by using appropriate stress and strain measures. All of our results have been obtained using Cauchy-Green strain and Cauchy stress.

$$\dot{W}^{p} = \sum_{\alpha} \left(\tau^{\alpha} - \omega^{\alpha}\right)\dot{\gamma}^{\alpha} \ . \tag{22}$$

Substituting relation (22) into equation (20) for the plastic work rate and solving equation for $\dot{W}^{p}$ we get the final form of the time independent plastic strain rate:

$$\dot{\gamma}^{\alpha} = \frac{\left(1-k\right)\left\langle \dfrac{\dot{W}}{s^{\alpha}} \right\rangle \left| \dfrac{\tau^{\alpha} - \omega^{\alpha}}{s^{\alpha}} \right|^{m} \left(\dfrac{\tau^{\alpha} - \omega^{\alpha}}{s^{\alpha}} \right)}{1 - k \sum\limits_{\alpha} \left| \dfrac{\tau^{\alpha} - \omega^{\alpha}}{s^{\alpha}} \right|^{m+2}} . \tag{23}$$

Note that equation (23) is already rate independent. The derivative of the shear strain, for each slip system is proportional to the total work density rate, and hence, the dependence on time will cancel out. This relation can be re-written in incremental formulation as follows:

$$\Delta\gamma^{\alpha} = \frac{\left(1-k\right)\left\langle \dfrac{\sum\limits_{i,j=1,3} \sigma_{ij} \Delta\varepsilon_{ij}^{total}}{s^{\alpha}} \right\rangle \left| \dfrac{\tau^{\alpha} - \omega^{\alpha}}{s^{\alpha}} \right|^{m} \left(\dfrac{\tau^{\alpha} - \omega^{\alpha}}{s^{\alpha}} \right)}{1 - k \sum\limits_{\alpha} \left| \dfrac{\tau^{\alpha} - \omega^{\alpha}}{s^{\alpha}} \right|^{m+2}} \tag{24}$$

Thus, we have formulated a rate-independent flow rule which automatically guarantees a unique selection of active slip systems at each time increment without any additional criteria and constraints. We also introduced one more model "weight" parameter $0 \le k < 1$. If the value of this parameter is close to zero, yield values change gradually as it usually observed during hardening. This corresponds to the case where the plastic strain rate is mostly defined by the total energy rate. In the limiting case of $k \to 1$ (in Eq. 23 or 24) there will be a sudden change in the plastic strain rate when $\tau^{\alpha} - \omega^{\alpha} = s^{\alpha}$, and, hence, s^{α} can be interpreted as a yield stress. Interestingly enough the gradual hardening behavior is correlated directly with the partial amount of dissipated energy which is proportional to the yield strain increment. Typical stress-strain curves with different values of parameter k are shown in Fig. 6 and one can see that regardless of the value of k, stress response converges to the same yield value.

In order to demonstrate that this rate-independent model provides accurate predictions we first consider the well studied example of single FCC crystal with the 'single-slip' crystallographic orientation $[\bar{2}36]$ as has been done in (Wu, Bassanni 1991 and Anand , Kothari 1996). We used model parameters for copper single crystals with noticeable latent hardening (Bronkhorst et al 1992) and compared our model predictions against the rate-dependent power model (Fig. 7). They are practically indistinguishable. Crystal lattice re-orientation behaves as expected (see Figure 7) going from the original triangle to the conjugate inverse triangle and then turning toward the (111) corner. The deformation starts with the single slip system $(111)[\bar{1}01]$ and continues with the activation of the second (conjugate) slip system $(11\bar{1})[011]$ which corresponds to the "bend" point on the inverse pole Figure 7. Predicted active slip systems are exactly what has been reported by Wu and Bassani (1991b). Our model calculations for corner orientations [001] and [111] also coincide with the known results predicting stable orientations and the corresponding 8 and 6 equally active slip systems specific for FCC crystals. This demonstrates that our rate-independent model provides reliable predictions for plastic deformation, guarantees the correct unique solution and can be used with the broad range of hardening laws. Having now a rate-independent model proven for classical hardening examples we can calibrate our parameters for Ni-based superalloy PWA1484 with relatively small latent hardening and use the calibrated model for the further analysis. Latent hardening of the Ni-based superalloy is very small as can be seen from the second curve in Fig. 7. The stress-strain relations for simple tension of the PWA 1484 specimens with <001> and <111> crystal orientations at 982 C is shown in Fig 8.

5. Computational results for cyclic loading LCF and TMF

We use our combined creep-plasticity approach to model cyclic loading conditions and to verify our simulation predictions against test results obtained on PWA 1484 Ni-based superalloy at both isothermal conditions (LCF tests) and out of phase (OP) TMF tests. The model parameters have already been calibrated during monotonic creep and plasticity tests over broad range of temperatures, nominal stresses and applied strain rates. During the reverse cycle the back stress is not yet steady and the absolute value of the effective stress $|\tau - \omega|$ reaches the critical value earlier than during the initial "forward" loading step resulting in the so-called Bauschinger effect. During reasonably fast strain controlled LCF, this effect does not play important role. In laboratory creep-fatigue interaction tests the dwell time has typically been limited to 5 minutes per cycle. In other words the specimen is deformed at a constant strain rate to some fixed strain and then is held at this strain for a dwell time causing stress relaxation. It is important to note that the cycle was symmetric ($R = -1$) and relaxation time was applied under both tension and compression conditions. The symmetry of cycles prevents ratcheting and provides the data to calibrate our models for strain and kinematic hardening evolution. During such a short time interval the creep process is essentially transient and our primary creep model plays the very important role in stress-strain predictions. Dislocations are nucleated under loading and dislocation cell structures dissolve whenever the back stress and the effective RSS have different signs (i.e. during unloading) and thus slowing the dislocation growth rate.

Results of our model comparison with test data are shown in Figs 9-12. Figure 9 (a and b) shows a comparison of model predictions against experimental data for <001> single crystal PWA1484 cyclically loaded up to 1% of strain amplitude at a temperature of 870 C. Due to strain hardening the hysteretic loop narrows as the number of cycles increases. The first loop (Fig 9a) is approximately as twice as wide the observed stress-strain relations at cycle number 30 (Fig. 9 b) where the cyclic loop is stabilized. Modeling results obtained for a $<\bar{1}23>$ single crystal orientation compared against test data are shown in Fig. 10 for isothermal conditions at 870 C, a strain range of 0.8% and for $R = -1$. We use the $<\bar{1}23>$ single crystal orientation since it initially has the single slip system $(111)[01\bar{1}]$ active. The loop is extremely wide due to the relatively low yield value for the single crystal along a single slip crystallographic direction and consequently the LCF life of this specimen is much shorter than the life of the specimen with a <001> crystallographic orientation. Similar tests performed on the specimens with the <001> crystallographic orientation show little or no hysteresis loop, at least within first thousand of cycles. It is also important to note that the LCF life of the highly symmetric <001> specimen was approximately 20 times longer than the results for loading along $<\bar{1}23>$ crystallographic direction. Comparison of the predicted response vs. test data demonstrates that our model provides good predictions for both the monotonic and the cyclic responses of a single crystal.

The dwell time during each cycle considerably reduces the fatigue life due to creep-fatigue interactions, which in turn multiplies the damage growth rate. Dwell-fatigue tests were performed at 982 C to the mechanical strain amplitudes of 0.5%. There are practically no plastic effects observed because the maximum stress is well below yield. Nevertheless the loop is wide open due to pure creep (actually, relaxation) effects. With an increase in the number of cycles the loop width slightly increases (about 20%) and stabilizes. The calculated and measured stress-strain curves at the cycle number 20 stress-strain curves are shown in Fig 11. The test fracture micrograph shows the striation lines and dimples due to inelastic effects (Fig 12). Fatigue cracking at high temperature takes place due to both cyclic controlled and time dependent processes. We have also analyzed the dwell-fatigue tests with loading along $<111>$ crystallographic direction performed at 871 C to the mechanical strain amplitude of 0.4%. Due to the high Young's modulus along the <111> orientation the stresses reach yield and the loop is wide open due to both plasticity and creep effects. Figure 13 illustrates the comparison between simulation results and test measurements for the cycle number 10. The comparison is excellent.

The results shown above demonstrate that the developed combined crystal rate-independent plasticity –creep model provides adequate prediction for monotonic as well as cyclic loading conditions. Both test and modeling indicate that the material damage per cycle depends on the stress-strain hysteresis loop width. Thus the interaction cannot be expressed as a direct sum of fatigue and creep induced damages.

TMF tests have been performed on cylindrical specimens with periodic temperature variations. The relatively long period thermal cycle has been defined by the necessity to ensure that there is no temperature gradient across the specimen section. The cycle time for continuous (non-dwell) tests varied from 2 to 3 minutes depending on the maximum specimen temperature. All the reported tests were out of phase (OP) TMF cycle (sometimes called Cycle I) and conducted in a strain control mode ($R = -1$) using servo-hydraulic machines. The test specimen was heated using a low frequency (10 kHz) induction generator. Tests were generally discontinued when the load on the specimen decreased by 70% in order to prevent damage to the extensometer and possibly the heating system. In order to cool the specimen at the required rate, forced air-cooling via an air blast directed on the specimen surface and/or through the center of the specimen was employed. TMF tests have been conducted over different temperature ranges, mechanical strains and crystallographic orientations. Temperature changes from 426 C to maximum temperature value varying (from one group of tests to another) in the range of 980 C - 1150 C. Mechanical strain range is chosen to be either 0.5% or 0.8%; dwell time at maximum temperature was either 5 or 30 minutes and specimens with three crystallographic orientation of (001), (111), and (123) have been tested.

During TMF cycling, latent hardening changes not only with strain but also with temperature. Therefore, the rate of change of slip resistance should be function of both slip rates and temperature rate. In order to predict latent hardening change with temperature and strain simultaneously the strain hardening rule has been modified as follows:

$$\dot{s}^{\alpha} = h_0 \left(1 - \frac{s^{\alpha}}{s^{*}} \right)^{p} \sum_{\beta} h^{\alpha\beta} \left| \dot{\gamma}^{\beta} \right| + \left(\frac{s^{*} - s^{\alpha}}{s^{*} - s_0} \right)^{p} \frac{ds_0}{d\Theta} \dot{\Theta} \qquad (25)$$

Note that the extra $\dot{\Theta}$ terms in equation (25) would force s^{α} to be an exact differential in γ^{α} and Θ if the absolute values were removed (for detailed discussion see Cassenti and Annigeri, 1989). Of course, for isothermal conditions the second term is identically zero.

In Figure 14 we compare the computational results with test measurements for OP, no-dwell tests of specimens with a (001) crystallographic orientation. The ratcheting (due to kinematic hardening) caused by inelastic effects at test temperatures is significant and slowly stabilizes after several hundred cycles. The shift of the stress-strain curves with cycle accumulation increases the maximum tensile stress at low temperature. Keep in mind that creep effects are suppressed at low temperature, and hence the major mode of energy dissipation becomes cracking. Thus, increasing the maximum value of tensile stresses with TMF cycles causes cracking at low temperature regime. Compression holds at high temperature (even at low stress level) increases relaxation and accelerates the ratcheting process. The low temperature maximum tensile stresses become much larger over fewer cycles in this case, and as a result the TMF life decreases. We compare the predicted stress-strain cycles with test data obtained for OP tests with 30 minutes dwell at high temperature and a small mechanical strain amplitude of 2.5E-3 in Figure 15. Hot compressive dwell noticeably increases the rate of ratcheting, since as the number of cycles increases the tensile stress at low temperature conditions becomes much more pronounced. Our model slightly over predicts initial ratcheting, but after about fifty simulated cycles, model predictions finally stabilize at stress values close to the observed ones as shown in Fig 16. Note that five minutes of compressive dwell time at 1040 C decreased TMF lives of PWA 1484 specimens in approximately 3 times and 30 minutes dwell reduced the TMF life 4 to 8 times depending on the strain range.

Crystallographic orientation also plays an important role in the overall elastic-plastic response of the TMF test specimen. A comparison of simulation results against test data for ($\bar{1}23$) oriented specimen is shown in Fig 16. One can see that the stress-strain response is quite different and we might expect that in this case the TMF failure would be driven by plastic dissipation rather than tensile stresses with no hysteresis, and subsequently the TMF life should be shorter. In this case the observed number of cycles to failure is more than 7 times smaller than in (001) oriented specimen.

We have completed a life prediction analysis of 41 specimens taken from different sets of OP TMF and LCF tests. The TMF peak temperature varied from 1040 °C to 1150°C (with and without dwell times at high temperatures) and the LCF tests conducted at constant temperatures varying from 815 C to 1040 C. The mechanical strain magnitude varied from 0.25% to 1%.

We use the results of the constitutive model described above and evaluate the rate of inelastic energy generation ΔW[4] per loading cycle:

$$\Delta W = \int_{cycle} \left[\sum_{\substack{slipsystems \\ \alpha=1,18}} (\tau^{\alpha} - \omega^{\alpha}) \dot{\gamma}^{\alpha} \right] dt \tag{26}$$

We conducted numerical simulations up to 20 cycles after which the cycle shape, size and positions stabilized. This is an idealization, especially for TMF tests, but as one will see from the analysis below, the error is reasonably small. The test data analysis shows that the value of the dissipated energy ΔW controls the life of the specimens. It is worth noting that the damage evaluated based on ΔW effectively accounts for the combined effect of fatigue and creep/plasticity through the width of the hysteresis loop and cannot be readily decomposed into a direct summation of the damages caused by fatigue and inelastic dissipation as widely used in engineering practice (i.e., Miner's rule). If crack propagation is controlled by a Paris law it is easy to show that the life is inversely proportional to the maximum principal stress to some power ($\sigma_{\max}^{m}$).

We begin by assuming the change in the damage over one cycle, ΔD, to vary according to

$$\Delta D = \left(1 + \kappa \Delta W\right)^{p} \left[\frac{\sigma_{\max}^{m}}{C_1} + \frac{\left(\Delta W \cdot D^{T}\right)^{k}}{C_2} \right] \tag{27}$$

where $\sigma_{\max}$ is the maximum principal stress, C_1, C_2, κ , $p, m,$ and k are constants. The quantity D^{T} is the thermal damage since we have observed that an increase of the maximum temperature by 100 °C (from 1040 °C to 1150°C) results in an approximately 3 times reduction of the TMF life depending on the strain range and other parameters. As has been already noted, high temperature dwell results in significant damage reducing the specimen life. Thermally-induced damage is defined by the energy generation rate and the effects of thermal-dwell effects that can be described with the help of the following "effective hot time" Arrhenius type correction:

$$D^{T} = A \int_{0}^{t} \exp\left(- \frac{Q}{k \Theta(\varsigma)} \right) d\varsigma \tag{28}$$

---

[4] Probably entropy generation rate, $\Delta S = \int_{cycle} \left[\sum_{\substack{slipsystems \\ \alpha=1,18}} (\tau^{\alpha} - \omega^{\alpha}) \dot{\gamma}^{\alpha} \right] \frac{dt}{\Theta(t)}$, has more physical meaning but predictions obtained based on each of these parameters are close and we use inelastic energy generation rate for the further explanations.

Note also that the specimen life is controlled by the energy dissipation, or in other words, damage initiation life varies with the variation of product $\left(\Delta W \cdot D^T\right)^k$ where the power $k < 1$ reflects the part of the dissipated energy contributes to the failure process.

We can convert equation (27) into an evolution law for the damage by considering the rate of change of state variables D, W and D^T to be the average over one cycle. Then, $\Delta D = \dot{D}\mathrm{T}_p$, $\Delta W = \dot{W}\mathrm{T}_p$ and $\Delta D^T = \dot{D}^T\mathrm{T}_p$ where T_p is the loading cycle period. The damage evolution equation now becomes

$$\dot{D} = \left(1 + \kappa \mathrm{T}_p \dot{W}\right)^p \left[\frac{\sigma_{\max}^m}{C_1 \mathrm{T}_p} + \frac{\mathrm{T}_p^{2k-1}\left(\dot{W}\dot{D}^T\right)^k}{C_2}\right] \tag{29}$$

If we now use the average over one cycle for the rates in W and D^T, then equations (29) does not vary over time and can be readily integrated. Based on the fact that damage $D = 0$ at time $t = 0$ and failure occurs at time t_f when the damage $D = 1$ and $t_f = N_f \mathrm{T}_p$, we can modify the equation (29) to the following form:

$$\frac{1}{N_f} = \left(1 + \kappa \Delta W\right)^p \left[\frac{1}{C_1 / \sigma_{\max}^m} + \frac{1}{C_2 / \left(\Delta W \cdot D^T\right)^k}\right]. \tag{30}$$

If we set $N_F = \dfrac{C_1 / \sigma_{\max}^m}{\left(1 + \kappa \Delta W\right)^p}$ as the number of cycles to failure due to elastic fracture only, and $N_R = \dfrac{C_2 / \left(\Delta W \Delta D^T\right)^k}{\left(1 + \kappa \Delta W\right)^p}$ as the number of cycles to failure due to inelastic rupture then equation (30) becomes

$$\frac{1}{N_f} = \frac{1}{N_F} + \frac{1}{N_R}. \tag{31}$$

It is important to note that some tests, especially those involving non-corner orientations, have extremely large values of ΔW and subsequently resulting in low lives predicted by standard methods of linear regression. The quantity $\left(1 + \kappa \Delta W\right)^p$ is included to accommodate this empirical observation. Equation (31) agrees with the work of Neu, R.W., and U. Sehitoglu (1989), and indicates that failure due to elastic and fracture of inelastic rupture are independent quantities.

Finally, we use regression to fit the coefficients C_1 and C_2, in the empirical life prediction formula. Once the fit is completed, the predicted lives are reasonably close with a standard deviation for a $\log_{10}$-normal distribution of approximately 0.25 which is well under one-half an order of magnitude. When the measured lives are plotted against the predicted lives the results are within a 2X corridor as can be seen in Figure 17 below.

7. Conclusions

The developed constitutive model has been implemented in the commercial finite element software ANSYS as a material user routine. The equations governing the mechanical response have been calibrated against experimental data. Such a calibrated model accurately predicts the crystallographic lattice rotation during large deformation, which is important during material processing as well as cyclic ratcheting, and is especially noticeable during LCF and TMF cycles.

Based on our modeling results and their comparison with experiments it is possible to conclude that the major deformation mechanisms of high temperature creep of Ni-based single crystal superalloy are octahedral {111}(110) and cube {001}(110) crystallographic slip. The increase of mobile dislocation density is the dominant mechanism for sigmoidal creep and can be adequately described using a two-body interactions formalism from chemical kinetics. We have also developed constitutive relations for primary creep using the concept of a threshold value to be proportional to the square root of the total dislocation density. The model predictions are very close to the test results. It is important to notice that creep strain rate and especially primary creep strain rates are very sensitive to the applied nominal stress values, making the primary creep negligible if the nominal applied stress is less than 2/3 of the yield value.

We have developed a new rate-independent crystal plasticity formulation that is designed for cyclic and non-isothermal loading conditions and can be readily applied to LCF/TMF over an extremely wide range of conditions. It combines the advantageous of rate-dependent and rate–independent formulation allowing for unique determination of the amount of shear along active slip systems at each time/strain increment. The approach is numerically robust and efficient, providing a working tool for low cycle fatigue (LCF) and thermo-mechanical fatigue (TMF) prediction analyses.

We verified our creep-plasticity approach by modeling cyclic loading conditions and comparing simulation predictions to test results obtained on PWA 1484 Ni-based superalloy at both isothermal conditions and at OP TMF tests. The quality of the prediction is very good. The analysis shows that the value of dissipated energy ΔW over the cycle controls the life of the specimens. Such a damage measure accounts for the combined effect of fatigue and creep/plasticity through the width of the hysteresis loop and cannot be decomposed into the direct summation of the damages caused by fatigue and inelastic dissipation as is widely used in engineering practice. From this point of view the creep-fatigue interaction is a crucial factor in decreasing the structural part life.

The combined theoretical-numerical-experimental study of the single crystal Ni-based superalloy PWA 1484 reported here increases our understanding of visco-plastic deformation in $L1_2$ systems; it holds substantial promise for future work. In particular, the model can be used to more accurately account for thermal-cyclic and for non-homogeneous transient temperature effects on structural component deformations and life prediction.

Summarizing, we have developed a viscous (creep) formulation and combined it with a new time independent formulation that accurately represents plastic deformations. We have developed a method that can simulate TMF, and have developed an empirical fit for the number of cycles to failure that effectively uses the dissipated energy (or equivalently the entropy).

Acknowledgements

The authors are grateful for support and funding from the United States Air Force Research Laboratory through contract # FA8650-07-C-5252 and to Dr. Andrew Rosenberger for his support and attention to this work.

References

Abdel-Karim, M.; Ohno, N.: *Kinematic Hardening Model Suitable for Ratchetting with Steady-State,* International Journal of Plasticity, 2000, Vol. **16**, p. 225-240.

Allan, C.D, Plasticity of nickel base single crystal superalloys. Ph.D. Thesis, MIT 1995

Anand L., Kothari M., (1996), A computational procedure for rate – independent crystal plasticity. J. Mech. Phys. Solids **44**, 525-558

Asaro R.J. 1983, Crystal Plasticity, ASME J. Appl. Mech. **50**, 921-934

Bari, S.; Hassan, T.: *Anatomy of Coupled Constitutive Models for Ratchetting Simulations*, International Journal of Plasticity, 2000, Vol. **16**, p. 381-409.

Bronkhorst, C. A., Kalidindi, S. R., and Anand, L.,``Polycrystalline Plasticity and the Evolution of Crystallographic Texture in F.C.C. Metals," Philosophical Transactions of The Royal Society, London **A, 341**, 443 -- 477, 1992.

Cassenti, B.N.,(1983), Research and Development Program for the Development of Advanced Time-Temperature Dependent Constitutive Relationships - Vol. 1 - Theoretical Discussion, NASA CR-168191.

Cassenti, B., and Annigeri, B. (1989), Thermodynamic Constraints on Stress Rate Formulations in Constitutive Models, Computational Mechanics, **6**, pp. 429-432

Chaboche J.L. (1986), Time-independent constitutive theories for cyclic plasticity. Int. J. Plasticity, **2**, pp. 149-188

Cowles, B. A. (1996) High cycle fatigue in aircraft gas turbines—an industry perspective, *International Journal of Fracture* **80**: 147-163.

Cuitino, A.M. and Ortiz M. (1993) Constitutive modeling of $L1_2$ intermetallic crystals. Material Science and Engineering, **A170**, pp.111-123.

A. Epishin; T. Link, (2004), Mechanisms of high-temperature creep of nickel-based superalloys under low applied stresses. Philosophical Magazine, 1478-6443, Volume **84**, Issue 19, Pages 1979 – 2000

Kalidindi, S.R., Bronkhorst, C.A., and Anand L., (1992) Crystallographic Texture Evolution during bulk deformation processing of f.c.c. metals. J. Mech. Phys. Solids **40**, 537-569.

Kalidindi, S.R., and Anand L., (1994), Macroscopic shape change and evolution of Crystallographic in pre-textured f.c.c. metals. J. Mech. Phys. Solids **42**, 459-490

Kocks, U.F., (1976) Laws for Work Hardening and Low-temperature Creep. *J. Eng. Mater.&Tech.* **98**, 76-85,

Krempl, E., C. H. Wells and Z. Zudans (1976) Workshop on Inelastic Constitutive Equations for Metals: Experimentation-Computation-Representation. RPI, Troy, NY

Levitin V., (2006) High Temperature Strain of Metals and Alloys. Wiley-VCH Verlag GmbH & Co KGaA, Weinheim 171 p.

Mughrabi, H., (1975), Description of the dislocation structure after unidirectional deformation at low temperatures, in Constitutive equations in Plasticity, Ed. A. Argon, MIT Press, Cambridge MA, pp. 199-251

Needleman A. (1988) Material Rate Dependence and Mesh Sensitivity in Localization Problems, *Computer Methods in Applied Mechanics and Engineering*, **67**, 69-85

Needleman A., (1989) Dynamic Shear Band Development in Plane Strain, *Journal of Applied Mechanics*, **56**, 1-9

Neu, R.W., and U. Sehitoglu (1989), Thermomechanical Fatigue, Oxidation, and Creep. Part II. Life Prediction, Metallurgical Transactions A: Physical Metallurgy and Materials Science, **20A**, pp. 1769-1783.

Nissley, D., Meyer, T., and Walker, K. Life Predictions and Constitutive Models for Engine Hot Section Anisotropic Materials, Pratt & Whitney, Report NAS3-23939, 1991

Peirce D**,** Asaro RJ and Needleman A. (1982) An analysis of nonuniform and localized deformation in ductile single crystals. Acta Metal**,** 30**:**1087-1119

Peirce, D. R. J. Asaro and A. Needleman (1983) Material Rate Dependence and Localized Deformation in Crystalline Solids, Acta Metal **31**, No 12, pp 1951-1976

T.M. Pollock and A.S. Argon (1992) Acta Metall., vol. **41**, p. 2253

Rae C.M.F. and R.C. Reed, (2007), Primary creep in single crystal superalloys: origins, mechanisms and effects, Acta Mater. **55**, p. 1067–1081.

J. R. Rice, J. W. Rudnicki, (1980) A note on some features of the theory of localization of deformation, Int. J. Solids & Structures **16** 597–605.

Rubeša, D. (1996), Lifetime prediction and constitutive modeling for creep-fatigue interaction, 152 p. Gebrüder Borntraeger, Berlin – Stuttgart

Sakaguchi, M. Okazaki, M. (2006), Thermo-Mechanical and Low Cycle Fatigues of Single Crystal Ni-base Superalloys; Importance of Microstructure for Life Prediction. *JSME, Series A*, **49**(3), pp. 345-354

J. Schröder, P. Neff and D. Balzani, A variational approach for materially stable anisotropic hyperelasticity, *Int. J. Solids Struct*., 42, 4352–4371, 2004.

Sugui T., Jinghua Z., Huihua Z., Hongcai Y., Yongbo X., and Zhuangqi H., (1999), Aspects of primary creep of a single crystal nickel-base superalloy, Materials Science and Engineering **A262** (No.1), pp. 271–278

Smith K. N., P. Watson and T. H. Topper, (1970), A stress-strain function for the fatigue of materials, J. of Materials JMSLA **5**, 767–775.

Staroselsky, A, and B. Cassenti (2006), Damage Accumulation at High Temperature Creep of a Single-Crystal Superalloy. In: Fracture of Nano and Engineering Materials and Structures. Proceedings of the 16th European Conference of Fracture. Ed. E. E. Gdoutos, Alexandropoulos, pp. 527 – 534

Staroselsky, A. Cassenti B., (2008) Mechanisms for Tertiary Creep of Single Crystal Superalloy, Mech. Time-Depend. Mater. **12**, 275-289

Stouffer, D.C., Dame, L.T., Inelastic Deformation of Metals, John Wiley & Sons, Inc. 1996

Valanis, K. C (1976), Constitutive Equations in Viscoplasticity: Phenomenological and Physical Aspects. AMD, Vol. **21**, ASME.

Walker, K. P. (1980), Representation of Hastelloy-X Behavior at Elevated Temperature with a Functional Theory of Viscoplasticity. Presented at ASME/PVP Century 2 Emerging Technology Conference, San Francisco, California, August 1980.

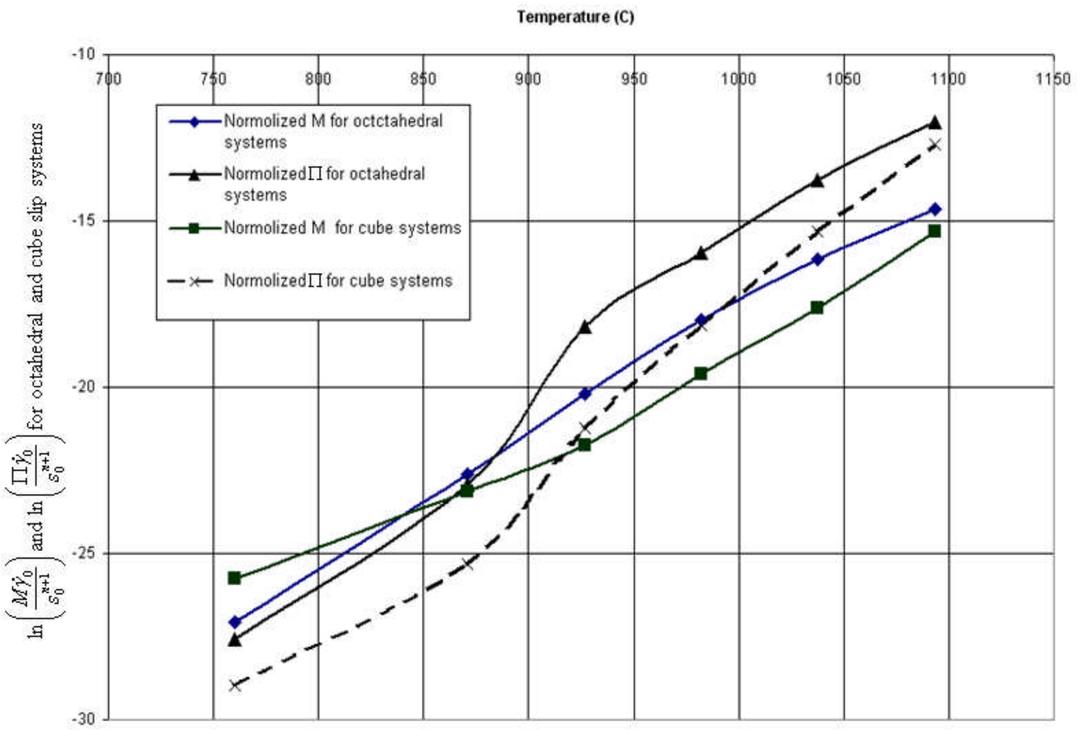

Figure 1. Normalized constants M and Π for dislocation densities evolution as functions of temperature.

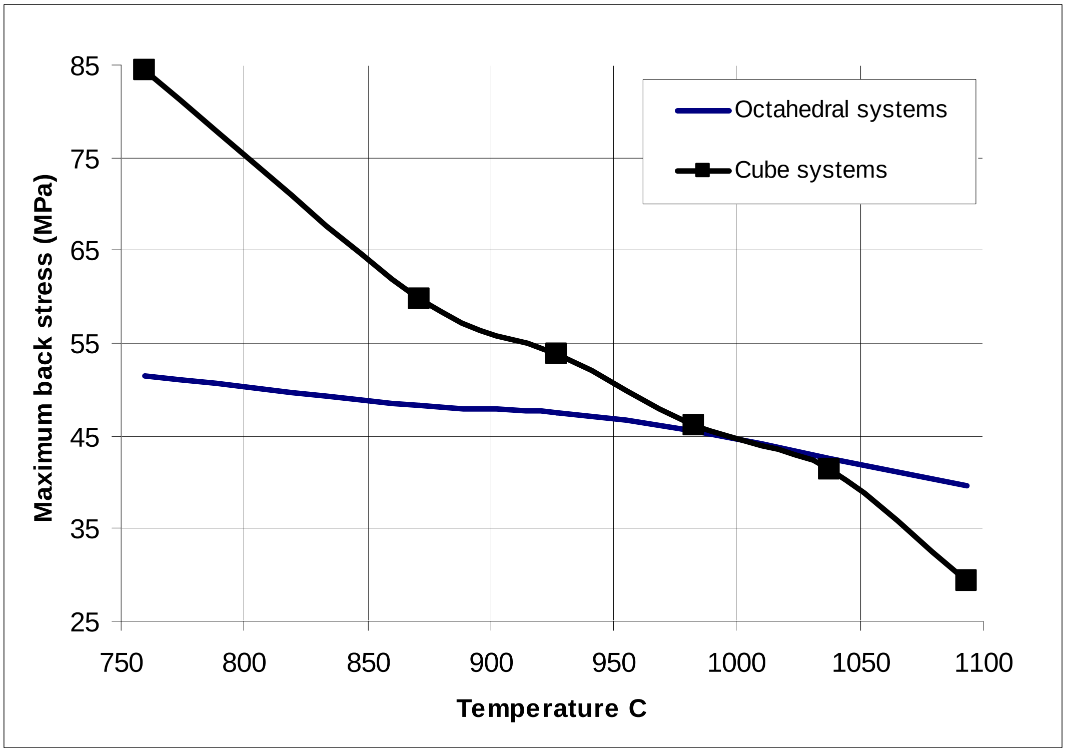

Figure 2. Variation of saturated back stress ω_∞ for octahedral and for cube slip systems with temperature.

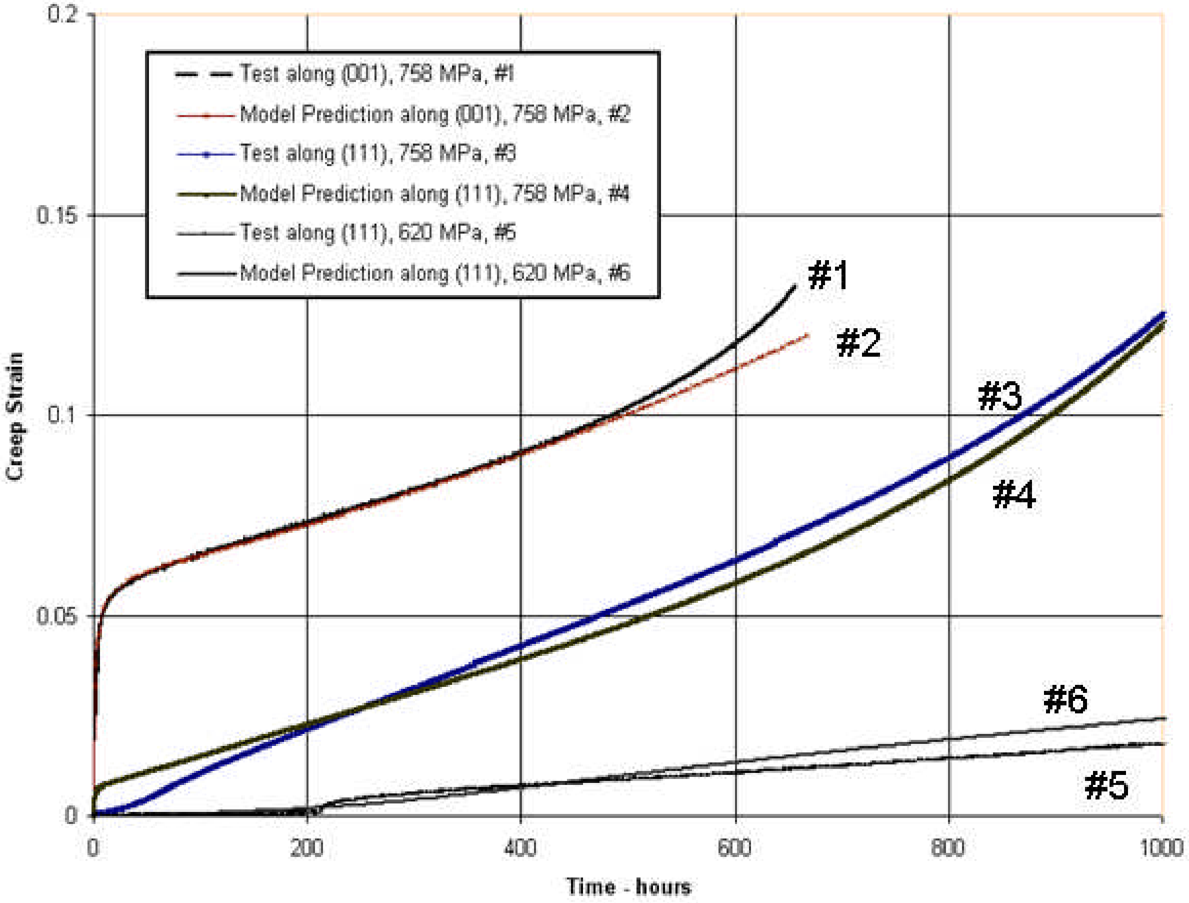

Figure 3. Model predictions and creep test results at temperature 760 C. Lines #1 and #2 are tests and simulation results correspondingly of creep along (001) crystallographic direction with nominal (initial) stress of 758 MPa. Lines #3 and # 5 are creep test results along (111) direction conducted at nominal stress levels of 758 MPa and 620 MPa correspondingly. Lines #4 is the simulation results for the test #3 and line #6 is the results of simulations for the test curve #5.

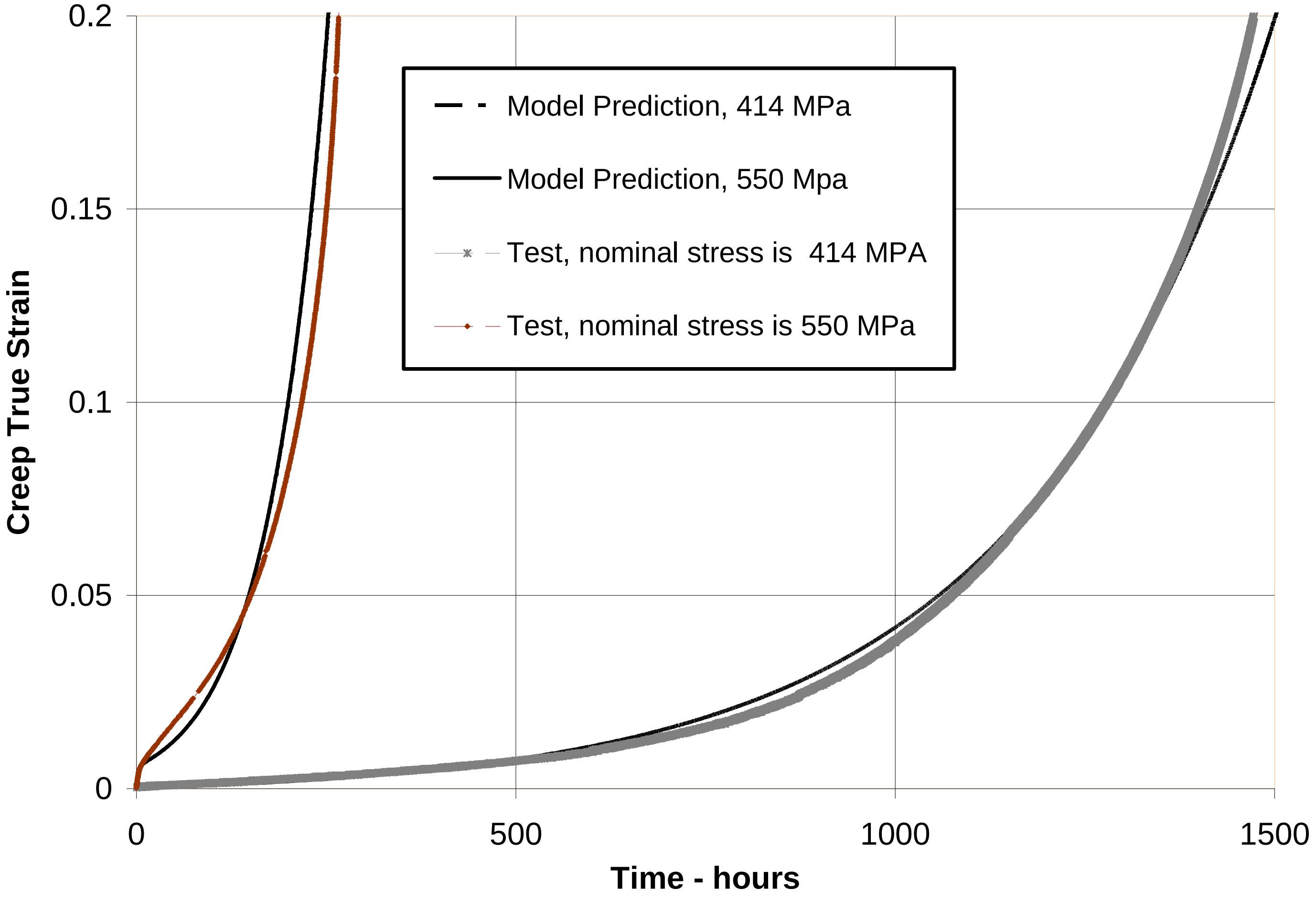

Figure 4. Model predictions and creep test results along (001) crystallographic direction at temperature 870 C and two nominal stress levels of 414 MPa (no primary creep region) and 550 MPa (with noticeable primary creep).

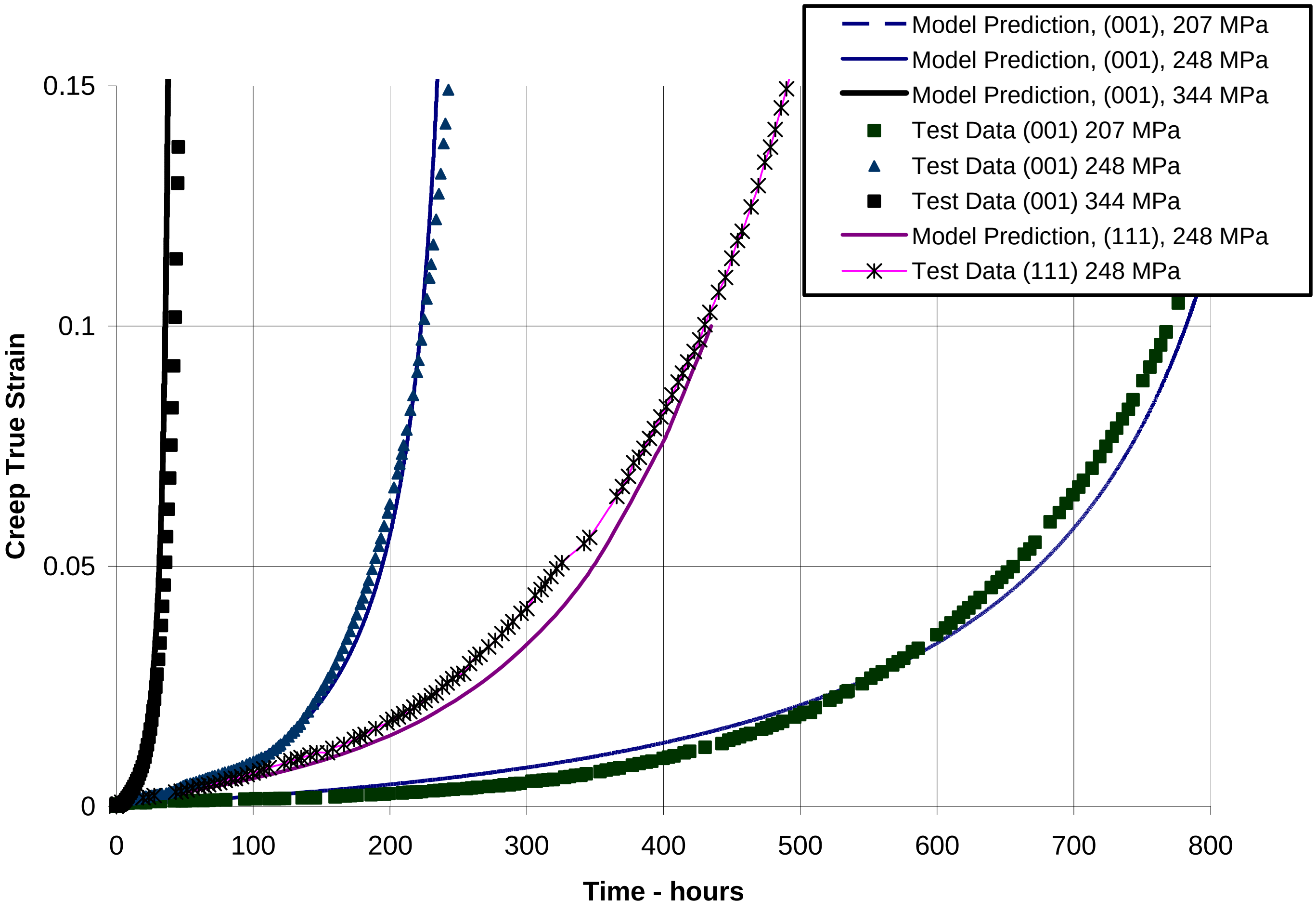
Model Prediction, (001), 207 MPa
Model Prediction, (001), 248 MPa
Model Prediction, (001), 344 MPa
Test Data (001) 207 MPa
Test Data (001) 248 MPa
Test Data (001) 344 MPa
Model Prediction, (111), 248 MPa
Test Data (111) 248 MPa
Creep True Strain
0.15
0.1
0.05
0
0
100
200
300
400
500
600
700
800
Time - hours

(a)

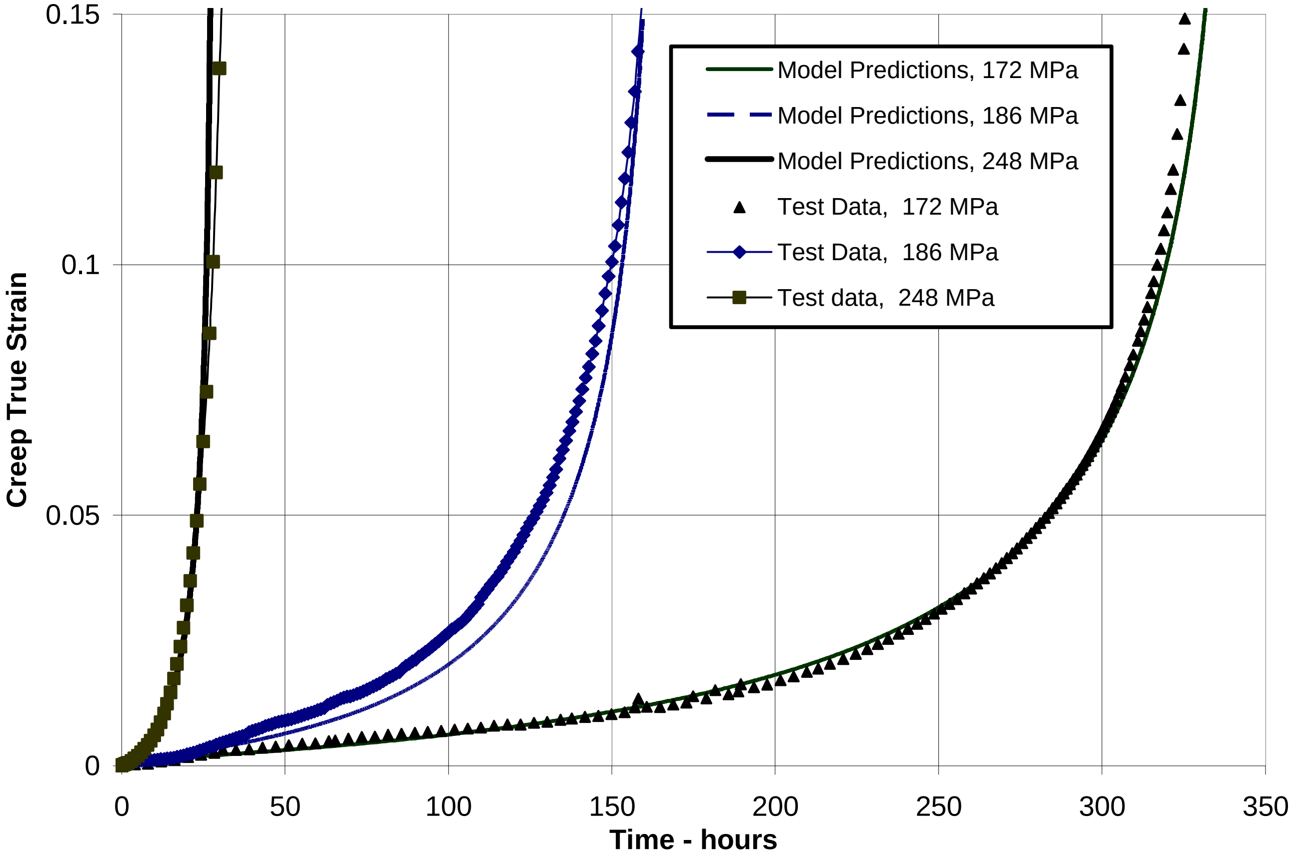

(b)

Figure 5. Creep Prediction vs. experimental data for (a) 982 C. Results correspond to three different nominal stress levels of 207 MPa, 248 MPa, and 344 MPa applied along (001) crystallographic direction and of 248 MPa applied along (111) direction.
(b) 1038 C. Results correspond to three different nominal stress levels of 172 MPa, 186 MPa, and 248 MPa applied along (001) crystallographic direction.

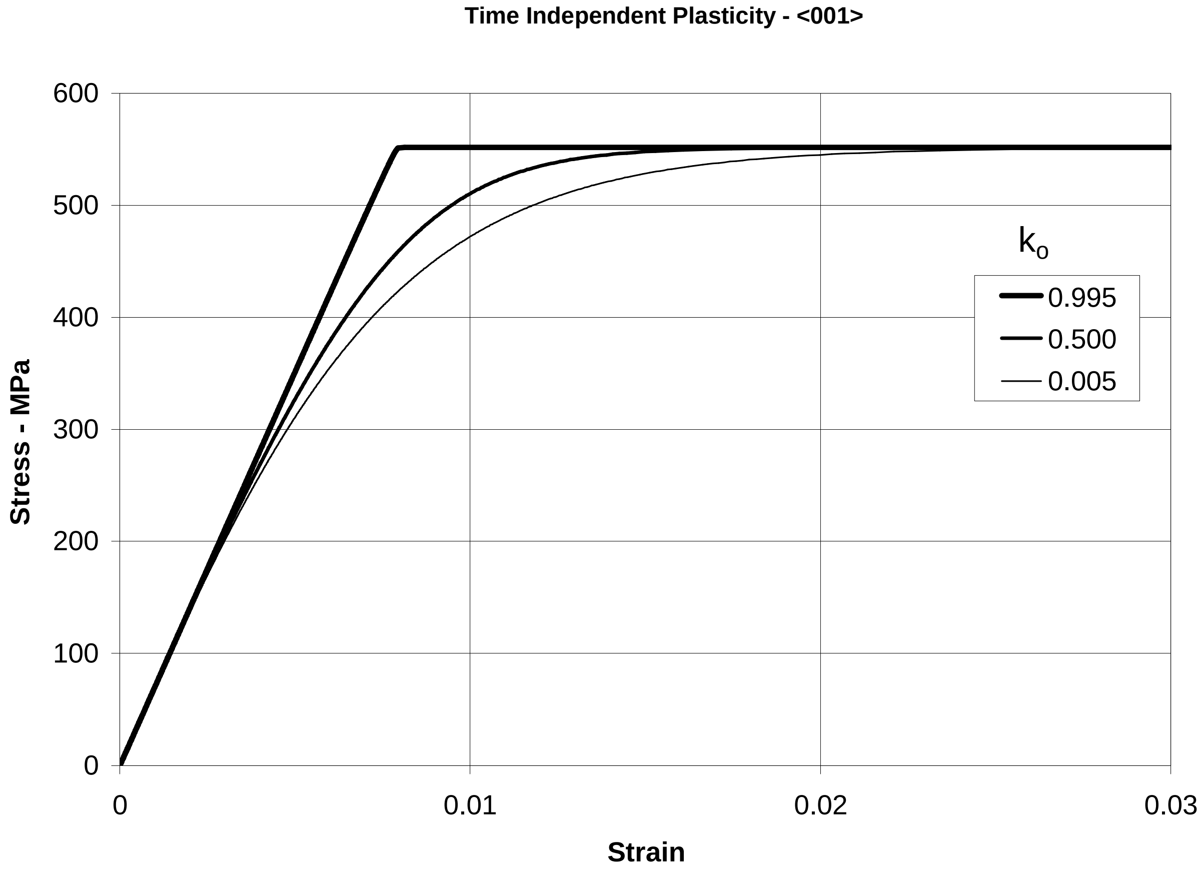

Figure 6. Typical stress-strain curves obtained with rate-independent model with different values of parameter k_0.

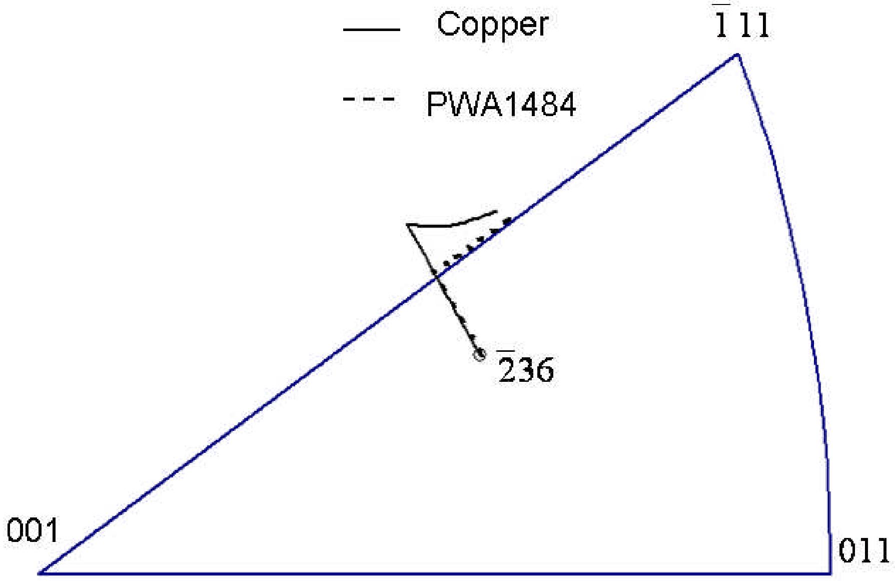

Figure 7.Results of single crystal re-orientation prediction for simple tension. Simulation results for copper with the high latent hardening demonstrate significant overshooting. Ni-based superalloy shows very little hardening, so crystal orientation evolution takes place close to the primary triangle border.

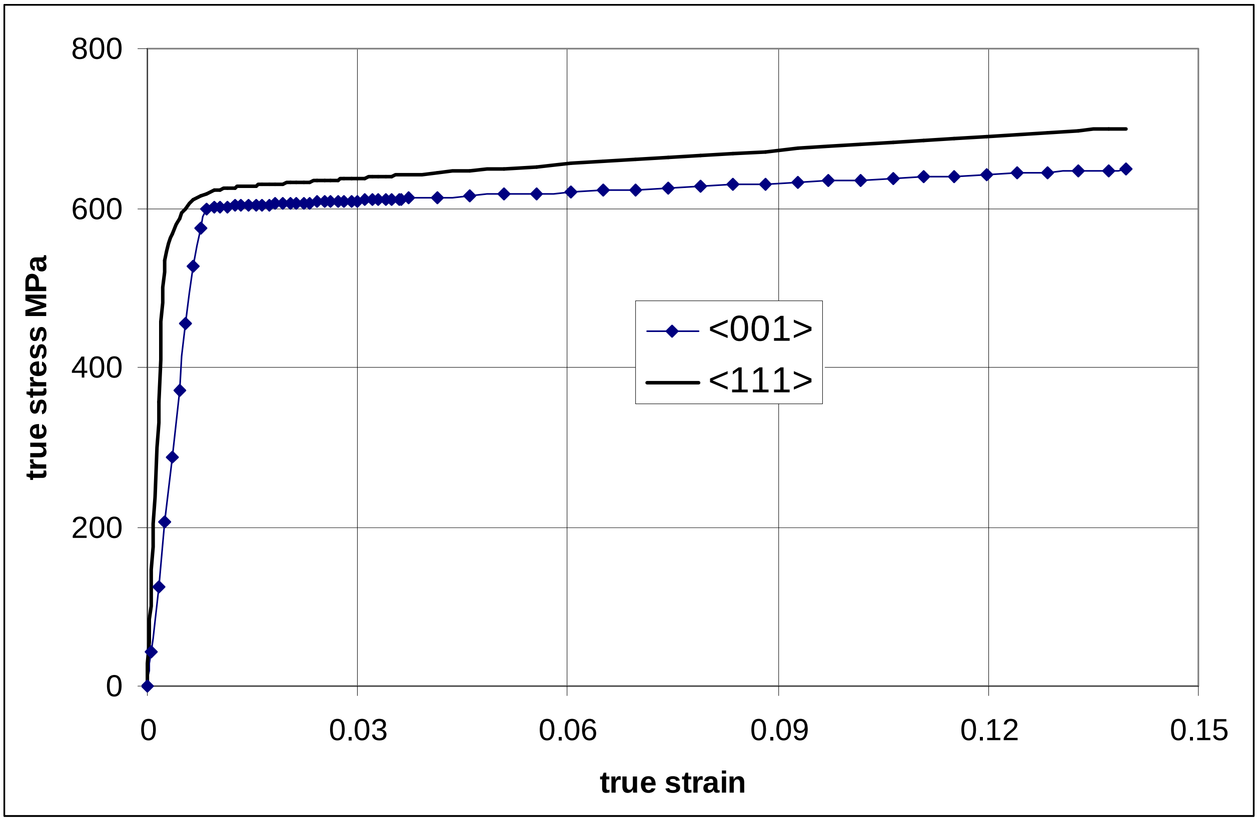

Figure 8. Typical calculated stress-strain relationship for simple tension along (001) and (111) crystallographic directions of PWA 1484

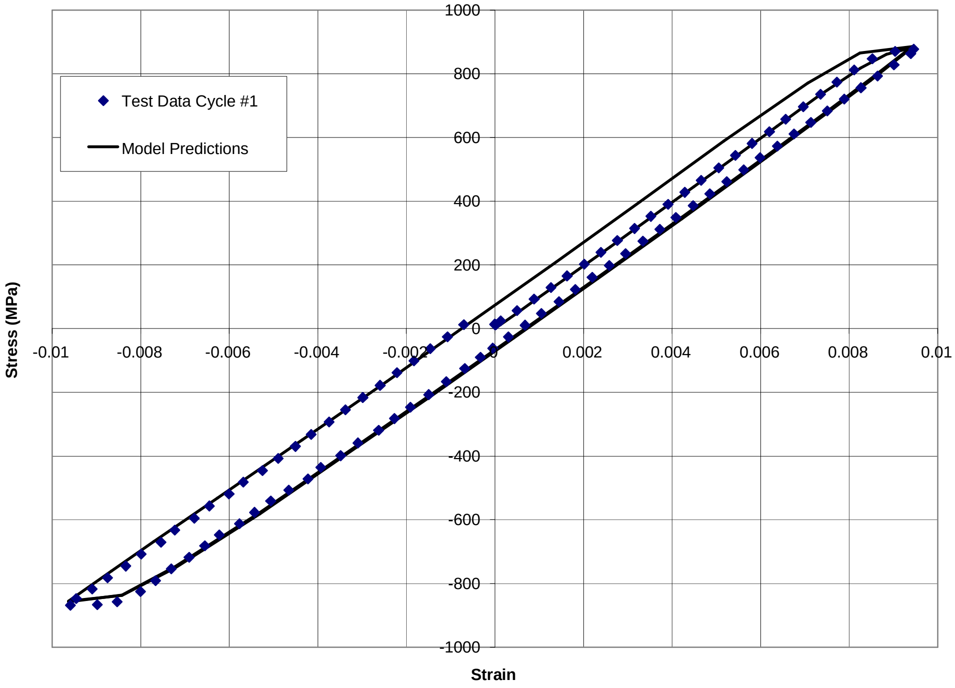

(a)

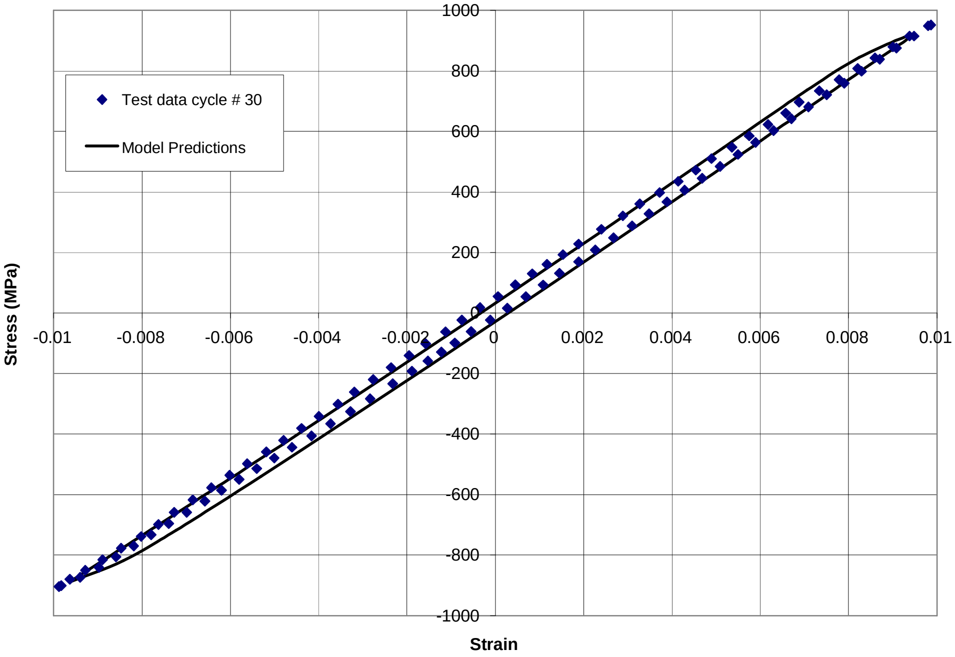

(b)

Figure 9. Predicted stress-strain relations against experimental data for strain-controlled cyclic test up to 1% strain along <001> crystallographic direction at 870 C. Results are shown for the first cycle (a), and cycle 30 (b).

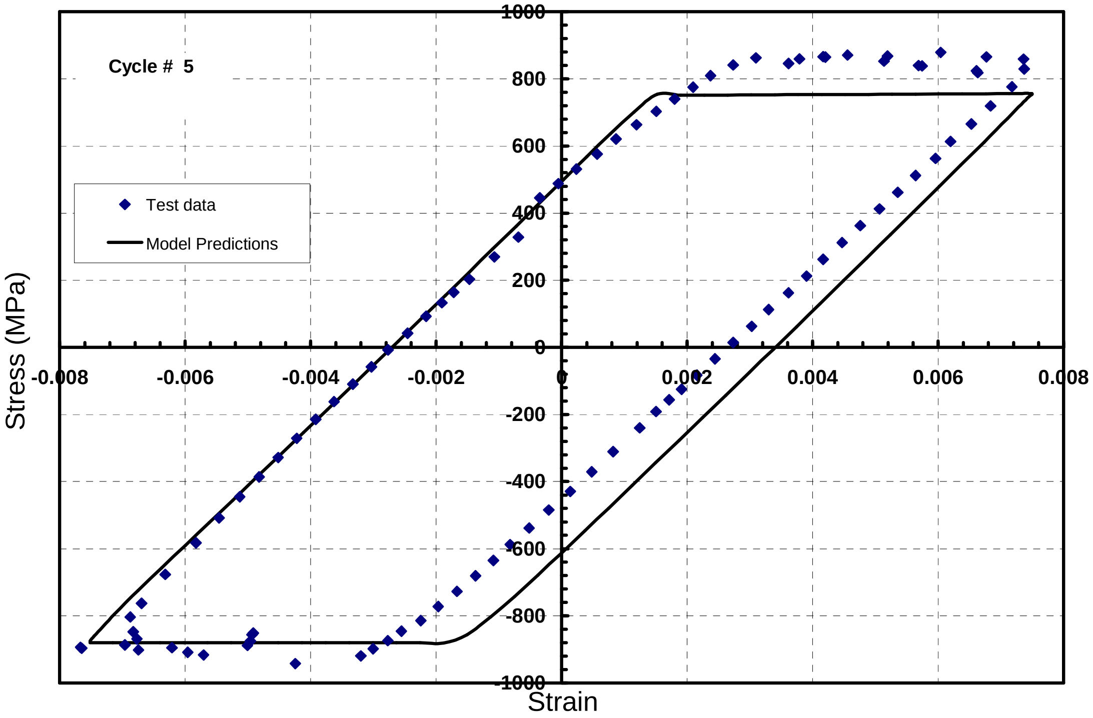

Figure 10. Predicted stress-strain relations against experimental data for strain-controlled cyclic test up to 0.8% strain range along $<\bar{1}23>$ crystallographic direction at 870 C.

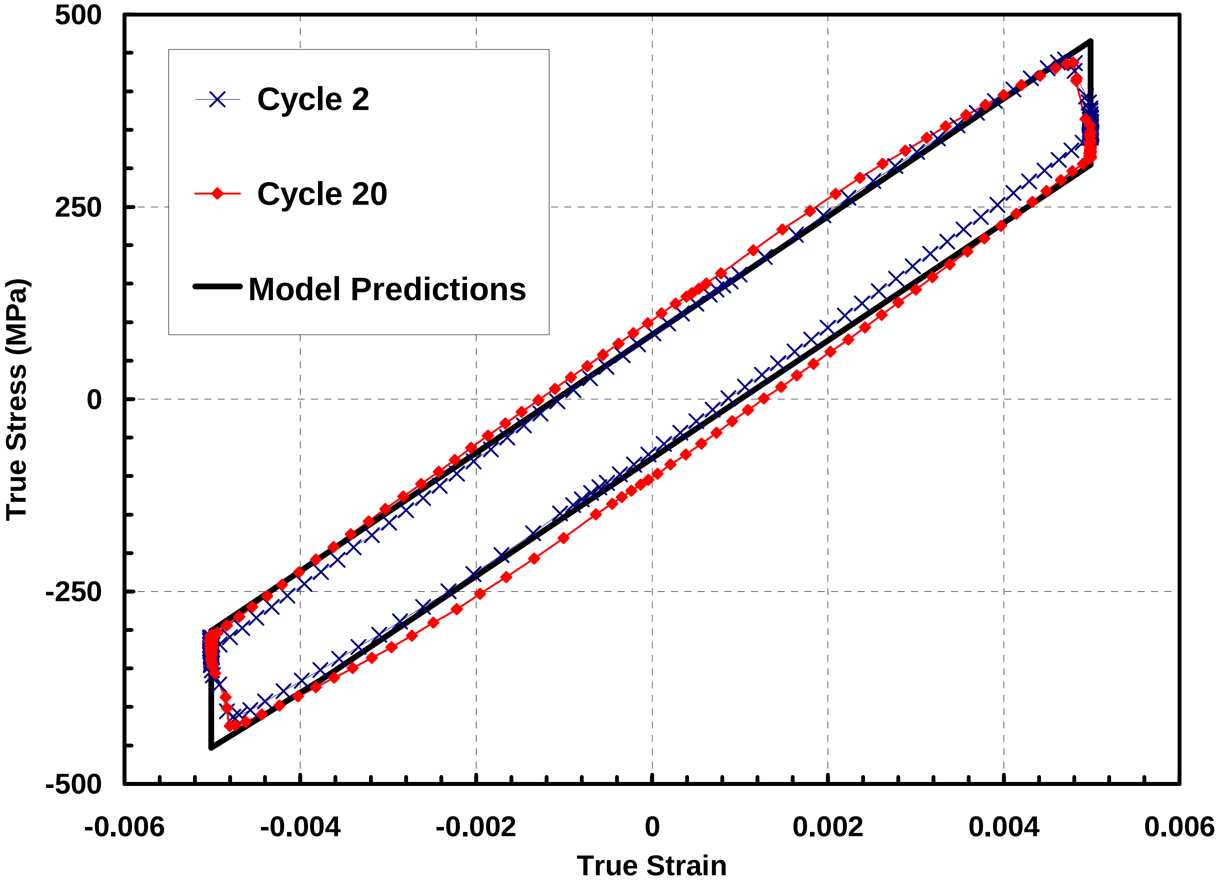

Figure 11. Predicted and measured cyclic stress strain curves for <001> oriented specimen at the temperature of 982 C, strain range of 1% with the symmetric cycle $(R = -1)$ and 5 min. dwell in both tension and compression.

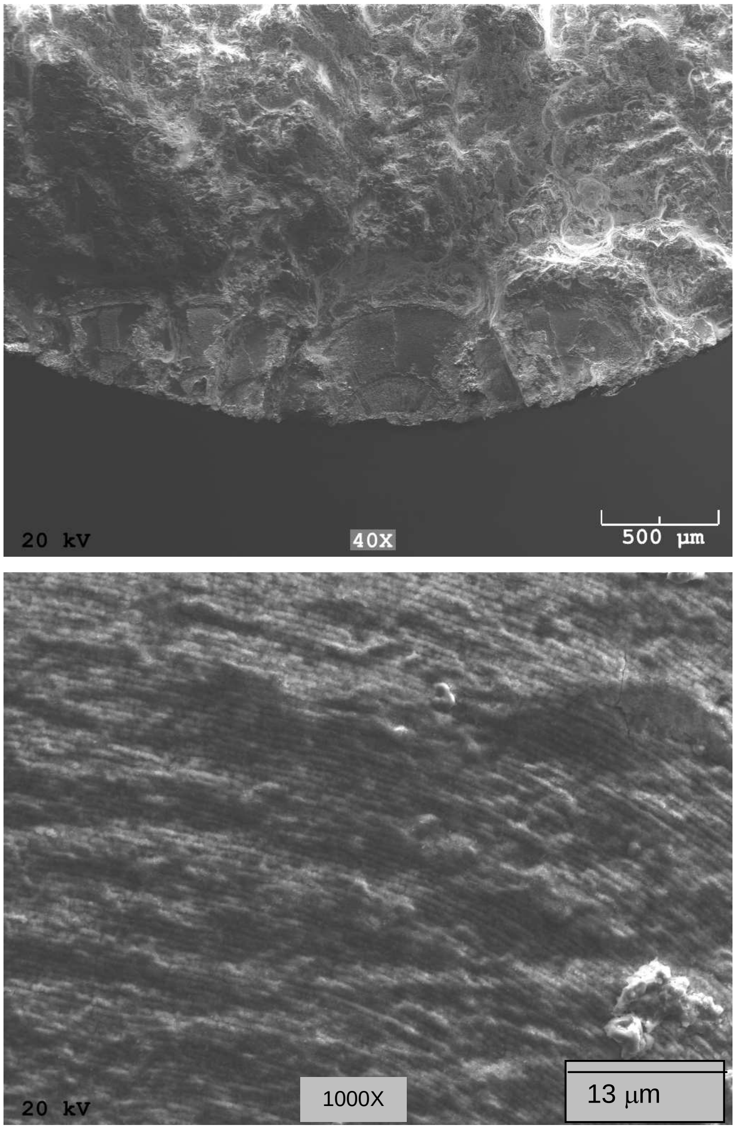
20 kV
40X
500 µm
20 kV
1000X
13 µm

Figure 12. Fracture micrograph for the cyclic test with 5 minutes dwell and strain range of 1% at 982 C.

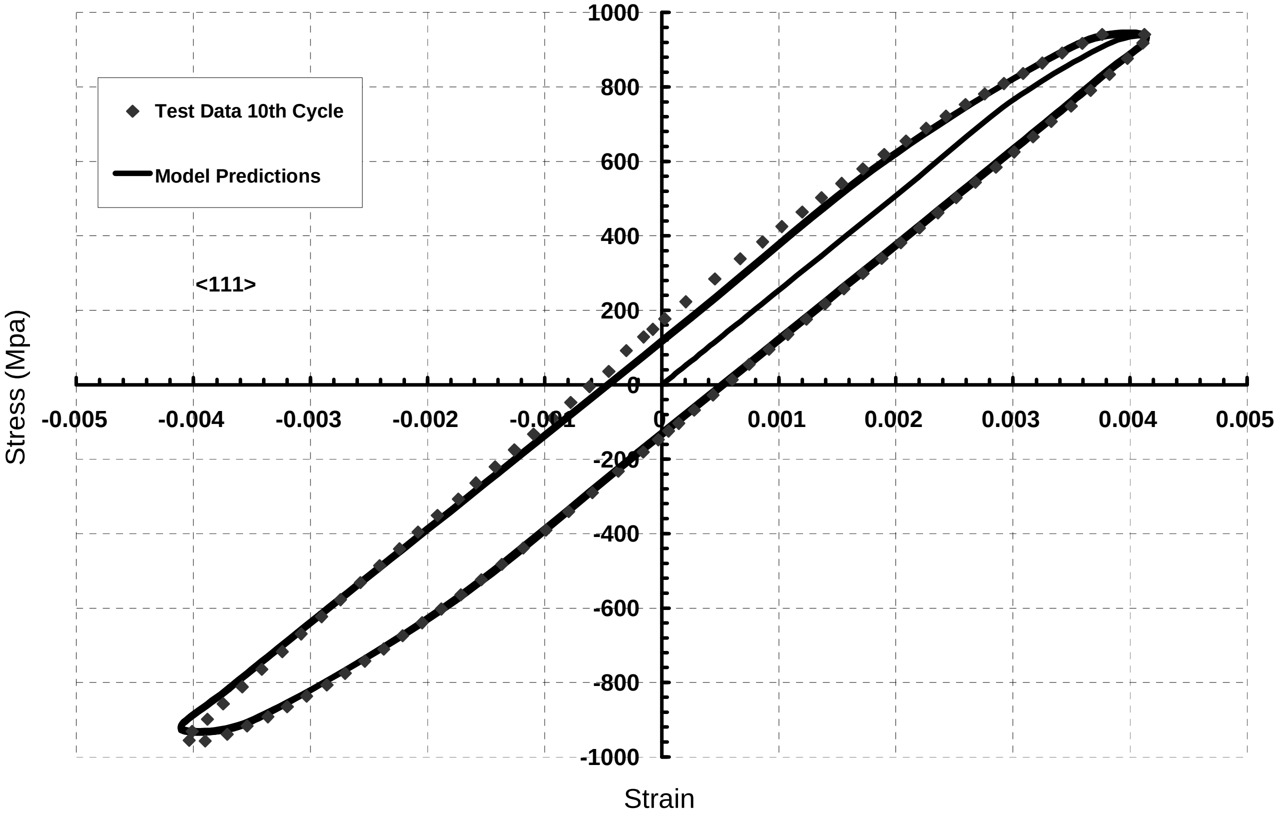

Figure 13. Predicted stress-strain relations against experimental data for strain-controlled cyclic test up to 0.8% strain range along <111> crystallographic direction at 870 C

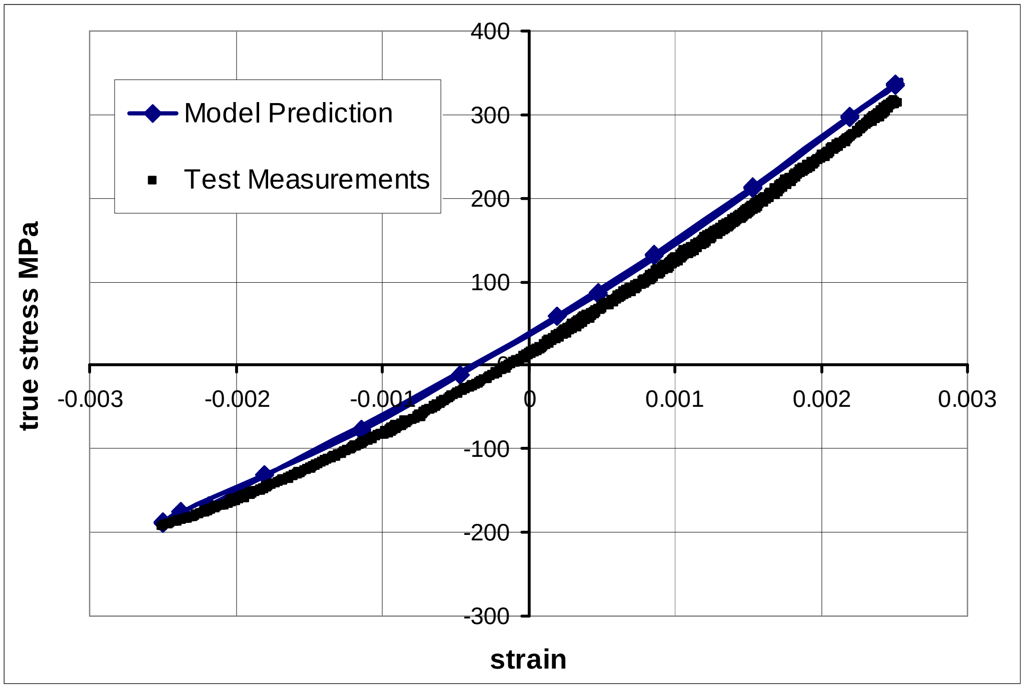

Figure 14. Predicted stress-strain curve against test data for out of phase thermal mechanical fatigue (OP TMF) test up to 0.25% strain range along (001) crystallographic direction at the temperature range from 427 C to 1038 C

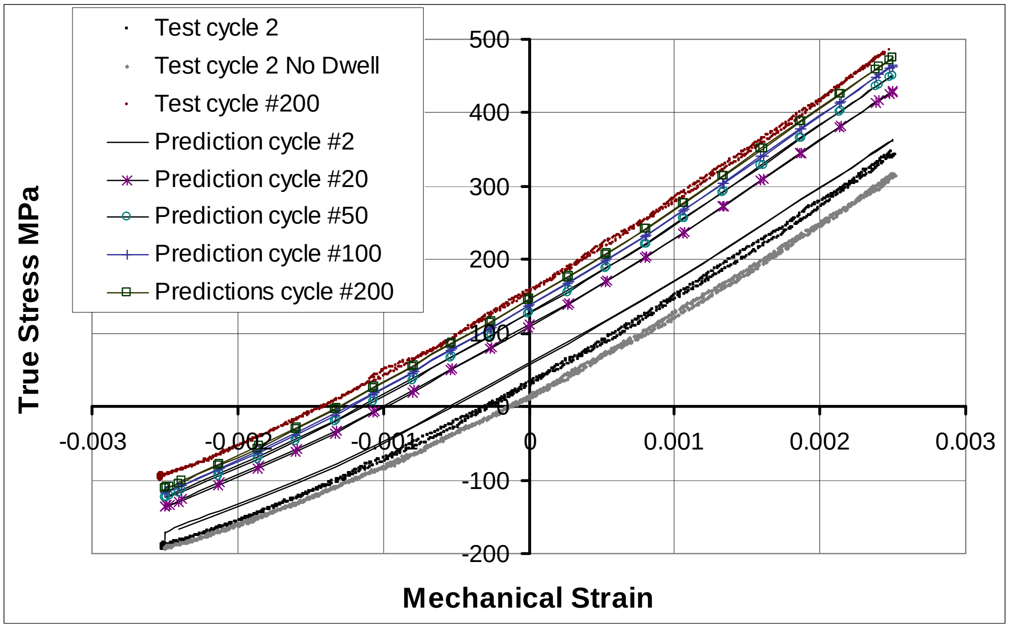

Figure 15. Predicted stress-strain curve against test data for out of phase thermal mechanical fatigue (OP TMF) test up to 0.25% strain range along (001) crystallographic direction at the temperature range from 427 C to 1038 C with hot dwell of 30 minutes

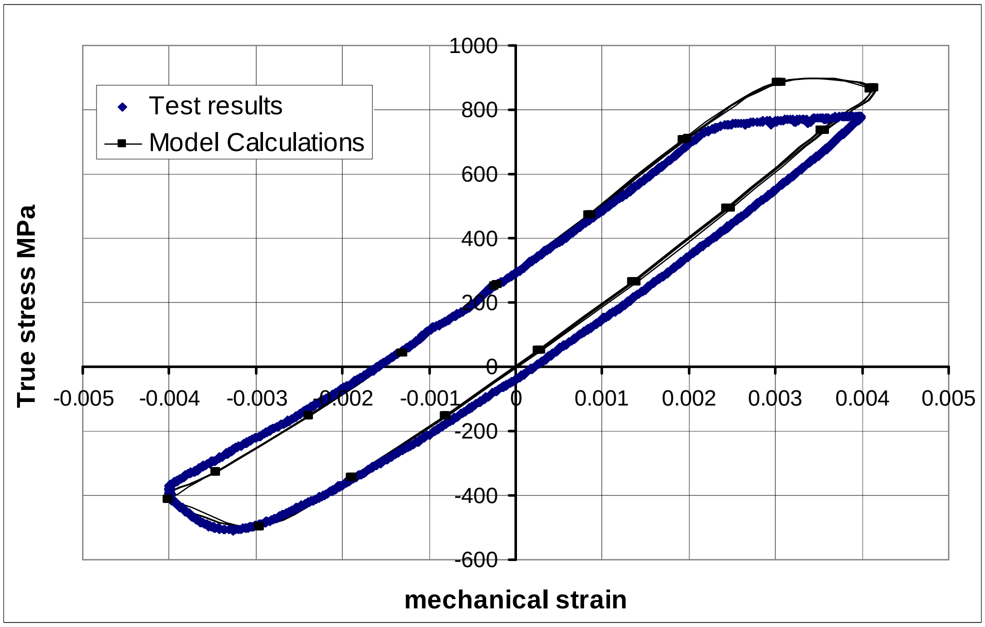

Figure 16. Predicted stress-strain curve against test data for OP TMF test up to 0.4% mechanical strain range along ($\bar{1}23$) crystallographic direction at the temperature range from 427 C to 1038 C

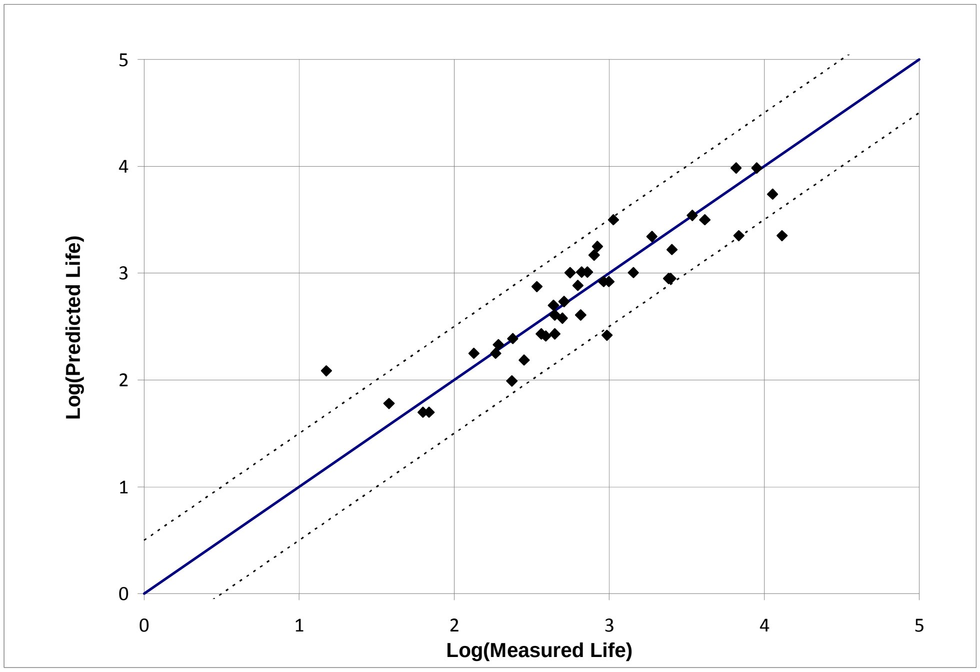

Figure 17. Life Prediction is within 2X interval against measured data for both OP TMF and isothermal LCF tests.